IMPLEMENTATION AND ASSESSMENT OF K-OMEGA-GAMMA TRANSITION MODEL FOR TURBULENT FLOWS

A THESIS SUBMITTED TO
THE GRADUATE SCHOOL OF NATURAL AND APPLIED SCIENCES
OF
MIDDLE EAST TECHNICAL UNIVERSITY

BY

SAMI KARABAY

IN PARTIAL FULFILLMENT OF THE REQUIREMENTS
FOR
THE DEGREE OF MASTER OF SCIENCE
IN
MECHANICAL ENGINEERING

MAY 2022

Approval of the thesis:

IMPLEMENTATION AND ASSESSMENT OF K-OMEGA-GAMMA TRANSITION MODEL FOR TURBULENT FLOWS

submitted by **SAMI KARABAY** in partial fulfillment of the requirements for the degree of **Master of Science in Mechanical Engineering Department, Middle East Technical University** by,

Prof. Dr. Halil Kalıpçılar
Dean, Graduate School of **Natural and Applied Sciences** _____

Prof. Dr. Mehmet Ali Sahir Arıkan
Head of Department, **Mechanical Engineering** _____

Assist. Prof. Dr. Özgür Uğraş Baran
Supervisor, **Mechanical Engineering, METU** _____

Examining Committee Members:

Assoc. Prof. Dr. Cüneyt Sert
Mechanical Engineering, METU _____

Assist. Prof. Dr. Özgür Uğraş Baran
Mechanical Engineering, METU _____

Assist. Prof. Dr. Ali Karakuş
Mechanical Engineering, METU _____

Assist. Prof. Dr. Onur Baş
Mechanical Engineering, TEDU _____

Assist. Prof. Dr. Hediye Atik
Mechanical Engineering, Atılım University _____

Date: 09.05.2022

I hereby declare that all information in this document has been obtained and presented in accordance with academic rules and ethical conduct. I also declare that, as required by these rules and conduct, I have fully cited and referenced all material and results that are not original to this work.

Name, Surname: Sami Karabay

Signature :

ABSTRACT

IMPLEMENTATION AND ASSESSMENT OF K-OMEGA-GAMMA TRANSITION MODEL FOR TURBULENT FLOWS

Karabay, Sami
M.S., Department of Mechanical Engineering
Supervisor: Assist. Prof. Dr. Özgür Uğraş Baran

May 2022, 58 pages

The transition from laminar flow to turbulence is challenging to model in CFD. Due to the complex nature of transition, it is neglected in CFD codes usually by assuming the flow is fully turbulent. However, this results in missing the fundamental characteristics of the flow and inaccurate predictions of the flow field. Although there are several transition models, most of them cannot be used in CFD simulations due to practical issues or low accuracy. Yet, some of these models are promising and candidates to be used in CFD simulations. In this study, Menter's $k-\omega-\gamma$ transition model is studied and applied to an open-source FlowPsi CFD solver. The main objective is to capture the transition mechanism in CFD simulations. The model is verified using the Klebanoff and ERCOFTAC flat plate cases and several 2D cases. Skin friction coefficient results are compared to experimental data. Results show that $k-\omega-\gamma$ transition model can predict laminar-to-turbulent transitions accurately.

Keywords: Transitional Flow, Transition Model, Intermittency, CFD, Flat Plate

ÖZ

K-OMEGA-GAMA GEÇİŞ MODELİNİN TÜRBÜLANSI AKIŞLAR İÇİN UYGULANMASI VE DEĞERLENDİRİLMESİ

Karabay, Sami
Yüksek Lisans, Makina Mühendisliği Bölümü
Tez Yöneticisi: Dr. Öğr. Üyesi. Özgür Uğraş Baran

Mayıs 2022 , 58 sayfa

Türbülanslı akıştan laminer akışa geçiş HAD analizleri için modellemesi zor bir fenomendir. Geçişin kompleks yapısı nedeniyle, HAD kodları genellikle akışın tamamen türbülanslı olduğunu varsayarlar. Fakat bu durum geçişli olan akışın modellenememesi ve yanlış sonuçlar elde etmeye neden olur. Birçok geçiş modeli olmasına rağmen çoğunluğu pratik nedenlerle veya düşük doğruluğa sahip oldukları için HAD analizlerinde kullanılamamaktadırlar. Yine de HAD analizlerinde kullanılmaya aday olan geçiş modelleri de vardır. Bu çalışmada Menter'in $k-\omega-\gamma$ geçiş modeli çalışıldı ve açık kaynak kodlu HAD çözücüsü olan FlowPsi koduna bu geçiş modeli eklendi. Çalışmanın ana amacı farklı mekanizmalarla oluşan geçiş fenomenini HAD analizleri ile çözümleyebilmektir. Modelin doğrulanması Klebanoff ve ERCOFTAC düz levha testleri ve 2B doğrulama testleri ile yapılmıştır. Yüzey sürüklenme katsayıları deneysel veri ile karşılaştırılmıştır. Sonuçlar $k-\omega-\gamma$ geçiş modelinin türbülanstan laminer akışa geçişi doğru bir şekilde tahmin edebildiğini göstermiştir.

Anahtar Kelimeler: Geçişli Akış, Geçiş Modeli, Kesiklilik, HAD, Düz Levha

To my family

ACKNOWLEDGMENTS

The author wishes to express his deepest gratitude to his supervisor Assoc. Prof. Dr. Özgür Uğraş Baran for his guidance, advice, criticism, encouragements, and insight throughout the research.

I would like to thank my dear colleagues.

I would also like to thank Roketsan Missiles Inc. for the encouragement that is shown through graduate program.

Lastly, I would like to thank my dear family that I am proud of.

TABLE OF CONTENTS

LIST OF TABLES

TABLES

LIST OF FIGURES

FIGURES

LIST OF ABBREVIATIONS

ABBREVIATONS

BCM	Bas Cakmakcioglu Model
CFD	Computational Fluid Dynamics
DNS	Direct Numerical Simulation
FVM	Finite Volume Method
LES	Large Eddy Simulation
RANS	Reynolds Averaged Navier Stokes
SA	Spallart Allmaras
SST	Shear Stress Transport
WCM	Walters Cokljat Model

LIST OF SYMBOLS

SYMBOLS

ρ	Density
E	Destruction Term
ν	Kinematic Viscosity
μ	Laminar Viscosity
P	Production Term
Re_V	Vorticity Reynolds Number
$Re_{\theta c}$	Critical Momentum Thickness Reynolds Number
$Re_{\theta t}$	Transition Onset Momentum Thickness Reynolds Number
Re_θ	Momentum Thickness Reynolds Number
Re	Reynolds Number
S	Strain Rate Magnitude
μ	Turbulent Viscosity
Tu	Turbulent Intensity
Ω	Vorticity Magnitude
γ	Intermittency
kL	Laminar Kinetic Energy
k	Turbulent Kinetic Energy
λ	Pressure Gradient Parameter
ω	Specific Turbulence Dissipation Rate

CHAPTER 1

INTRODUCTION

The transition from laminar to the turbulent regime, called laminar-to-turbulent transition, is a complex and compelling phenomenon in engineering studies. Because of its significant impact on the performance of many real-life applications, including aircraft, wind turbine, and turbomachinery applications, the laminar-turbulent transition has been the subject of theoretical, experimental, and computational studies. A laminar flow with an ordinary, streamlined velocity profile evolves into a turbulent flow characterized by unpredictable variations in several flow variables, such as velocity and pressure. The leap between these very different flow regimes is called the transition. One of the main differences between the laminar and turbulent flows is their very different skin friction. Therefore, for an accurate drag prediction, transition onset should be modelled to separate these regions. As a result, if the transition can be modeled and predicted accurately, many real-life applications can be designed more precisely.

The complex nature of transition hinders obtaining accurate predictions of transient flows with an analytic approach. However, with computers' ever-increasing calculating capability, it's become more feasible to examine the transition process using computational fluid dynamics, which allows for numerical modeling of the phenomena. With the increasing availability of high-performance computing (HPC) resources, there has been a movement in modeling trends toward computations using Large Eddy Simulation (LES) and Direct Numerical Simulation (DNS). Although these numerical approaches have been proved to attain high accuracy, they need a large amount of computing power seldom accessible in everyday simulations. As a result, less resource-intensive techniques, like those based on the RANS method, remain feasi-

ble choices, particularly for general-industrial CFD simulations.

Much effort has been made to numerical modeling of the transition during the last twenty years, resulting in a wide range of methodologies for RANS-based simulations. The first attempt at RANS-based model transition modeling is low Reynolds number turbulence models. Although this approach can give acceptable predictions for transition, the usage of these models is limited. Following this first approach, a new family of transition models based on nonlocal variables is developed. Although they were promising, implementing the nonlocal transition models into general-purpose CFD codes is not practical. Lately, transition models based on local variables have been introduced [1, 2, 3]. Transition models use the local variables to attract attention as they can give reasonably accurate solutions. The Langtry-Menter $\gamma - Re_\theta$ model [4] is the first approach to modeling transition based on the local variables. The general functionality of the Langtry-Menter $\gamma - Re_\theta$ model has increased with additional model modifications to accommodate for the effects of surface roughness and crossflow situations. However, this model is very complex, making it challenging to implement for different turbulence models and fine-tune for specific flow scenarios. The Langtry-Menter transition model also lacks Galilean invariance, an essential property for generic CFD simulations.

Lately, Menter et al. proposed [5] a new local correlation-based transition model based on a single transport equation and may be thought of as an improved version of the $\gamma - Re_\theta$ model. The new model benefits from the simpler formulation. Also, this model is Galilean invariant.

1.1 Transition Phenomena

The boundary layer is defined as the flow region adjacent to a bounding surface where viscous effects are significant. The boundary layer has two flow regimes, each with distinct characteristics: laminar and turbulent. Figure 1.1 depicts a boundary layer development across a plate to illustrate the relationship between these two distinct flow regimes through a transition region.

When uniform velocity fluid reaches the upstream of the plate, a laminar boundary

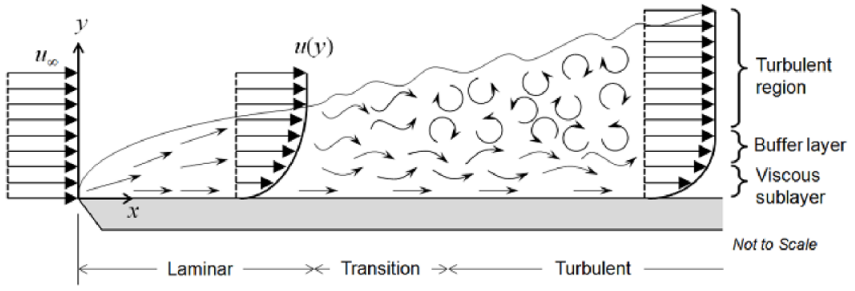

Figure 1.1: Transition Phenomena [6]

layer begins to form. The laminar region consists of a streamlined and smooth velocity profile near the surface. Disturbances in the flow field appear after a certain distance, indicating the onset of the transition zone. The whole flow field ultimately breaks down into a completely turbulent flow characterized by random changes in flow variables as oscillations and chaotic movements grow.

The fundamental governing parameter separating viscous flow regions is a particular dimensionless term, the Reynolds number. The Reynolds number indicates whether the flow is laminar or turbulent. It is defined as the ratio of inertial forces to viscous forces and formulated locally for the flat plate as follows.

$$Re_x = \frac{\rho U_\infty x}{\mu} = \frac{inertial forces}{viscous forces} \tag{1.1}$$

A low Reynolds number indicates a laminar boundary flow, whereas a high Re indicates a turbulent flow. Threshold Reynold numbers that separate whether the flow is laminar, turbulent, or transition are provided empirically. As previously stated, the laminar and turbulent flow regimes differ significantly. Hence, the point of transition influences the overall properties of the flow. In contrast to the turbulent boundary layer, the thinner laminar boundary layer exhibits less skin friction, and hence the total drag of the surface reduces. The turbulent flow has more momentum and maintains a higher velocity at the boundary layer, where it rapidly decelerates in a very thin zone. This large gradient of the fluid velocity adjacent to the wall in turbulent flows is the reason for greater skin friction. Laminar and turbulent flows have completely different heat transfer characteristics besides drag force. Due to the increased mixing in the turbulent flow, significantly higher heat between the fluid and the bounding surface

is observed. Laminar modeling underestimates skin friction drag and heat transfer, whereas fully turbulent modeling overestimates both. Thus, transition modeling is required if the laminar to turbulent transition occurs in the actual flow.

1.2 Transition Mechanisms

The transition can occur through different mechanisms due to a variety of reasons. Freestream conditions, turbulence intensity, and surface roughness can be given as examples. Generally, the primary modes are natural, bypass, and separation-induced transitions. Wake-induced and shock-induced transitions are classified as secondary transition modes [7]. In this part, different modes of transition are explained.

1.2.1 Natural Transition

When the flow interacts with a surface, a boundary layer develops. At the beginning of the boundary layer, flow is considered stable and laminar. As the flow moves on, instabilities occur in the boundary layer. When the flow reaches the critical Reynolds number, Tollmien-Schlichting waves are produced. The instabilities in the boundary layer amplify, and three-dimensional unstable waves start to grow. Turbulent spots are formed in the boundary layer due to amplified instabilities and fluctuations. Finally, with the growth and convection of the turbulence spots, the flow becomes fully turbulent [7][8].

If the transition occurs through these stages, it is called natural transition. The natural transition is the primary mechanism observed in zero pressure gradient flat plate transition. If the surface interacting with the fluid is smooth and freestream turbulence intensity is lower than 1%, the natural transition is the expected transition mode.

1.2.2 Bypass Transition

If the freestream turbulence level is larger than 1%, natural transition stages are bypassed, and turbulent spots are produced directly. In this mode, called bypass transi-

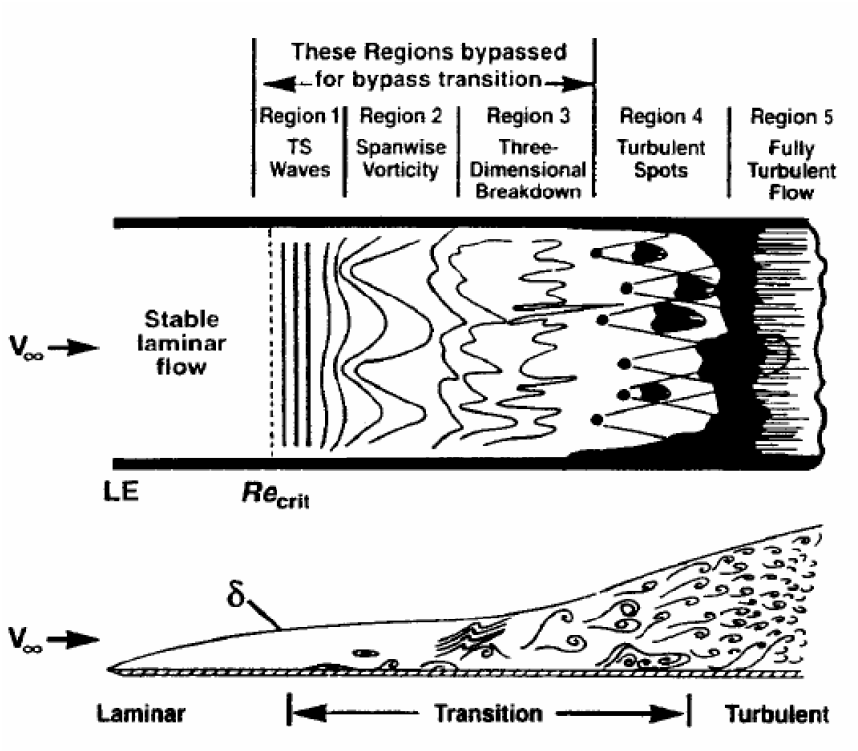

Figure 1.2: Natural Transition Mode [6]

tion, linear stability theory fails, and no Tollmien-Schlichting waves are formed [9]. Besides the freestream turbulence level, bypass transition can occur if the surface is rough. Similarly, favorable pressure gradients can also be a reason for the bypass transition mode.

1.2.3 Separation Induced Transition

When the flow separates, the transition may occur in the shear layer. In this mode, a laminar separation bubble can be formed on the surface, resulting in the flow reattachment. This mode contains all stages of the natural transition. According to the freestream turbulence level, the size of the separation bubble changes. Similarly, if turbulence intensity is low enough for the natural transition, Tollmien- Schlichting waves can be seen in the boundary layer.

1.2.4 Wake Induced Transition

This transition mode can be observed on periodic unsteady turbulent wakes passing over blades or airfoils [8][10]. Turbulent wakes disrupt the laminar boundary layer when they impinge the wakes, and turbulent spots propagate downstream. Although not much is known about the wake-induced transition, this mode resembles bypass transition due to direct turbulent spot formation.

1.2.5 Reverse Transition

Reverse transition or relaminarization refers to the transition from turbulent to laminar. The acceleration parameter is given as follows.

$$K = \frac{\nu}{U^2}\frac{dU}{dx} \tag{1.2}$$

This parameter is used to distinguish the reverse transition. Experiments show that if K is larger than $3x10^{-6}$, the reverse transition occurs. Acceleration results in the streamwise vortex lines stretching and dissipating due to viscosity [7, 8]. Thus, turbulence energy turns into heat, and flow becomes laminar. Moreover, another transition (retransition) to turbulence can occur after relaminarization.

1.3 Transition Modelling

It is possible to consider transition models according to their level of sophistication. The most basic model is the e^N model [12] The model is based on the linear stability theory and is often used for low turbulence level flows. The main assumptions of this theory are that flow is two-dimensional and steady, and the boundary layer is thin. Therefore, the e^N model is limited to the flows that satisfy those assumptions. A velocity profile is required as it is used to calculate the local instability amplification rates after the first instability along each streamline. The model predicts the transition if the amplification rate is higher than a threshold. The treshhold is based on observations and experiments. However, the e^N model cannot model the transition region

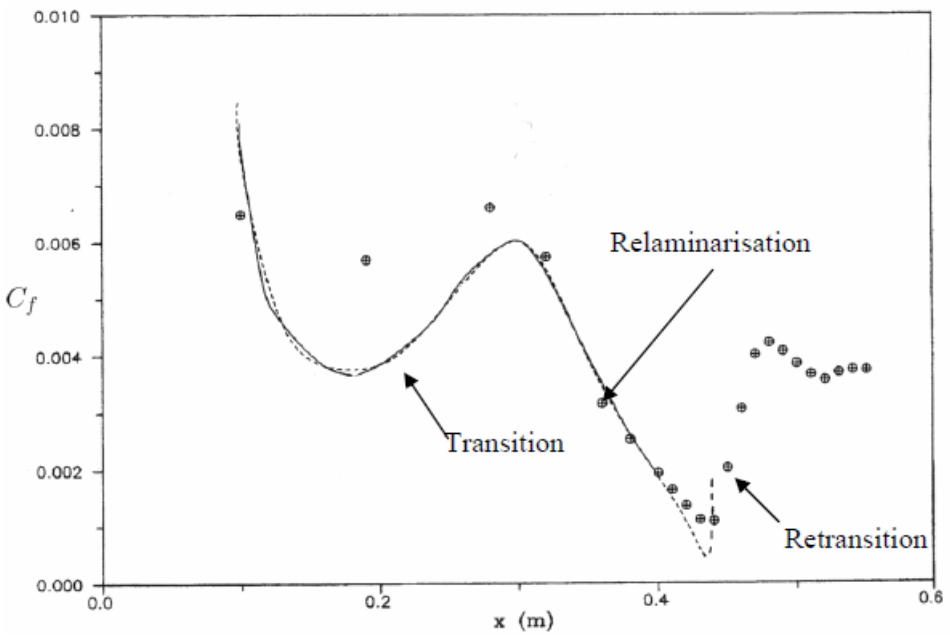

Figure 1.3: Relaminarization and Retransition[11]

[13].

Following the e^N model, low Reynolds Number turbulence models, which are more advanced compared to the e^N model, are introduced [14]. In these models, wall damping functions are modified to capture the transition effects. These models rely on turbulence diffusion from the freestream into the boundary layer to anticipate the transition onset. Low Reynolds Number turbulence models are generally used for bypass transition flows. However, they are unreliable since they are not sensitive to pressure gradients. Furthermore, simulations of separation-induced transition can have convergence problems using these methods [15].

Next, a group of more advanced and more complex transition models called correlation-based transition models are formulated [16]. The main idea is to blend the laminar and turbulent regions by introducing a new variable, intermittency [4, 5, 11]. Intermittency could be defined as the probability that the flow is turbulent or not. Detailed information about the intermittency concept is given in the following chapter. These models try to model the intermittent character of turbulence resulting from the fluctuations in the flow field. A new set of algebraic or partial differential equations are coupled with existing turbulence models [4, 17, 18, 19]. In those equations, constants derived from experiments and observations are used. It is convenient to group these

models according to whether they use local or nonlocal flow variables [16].

1.3.1 Models Depending on Nonlocal Flow Variables

These models calculate the momentum thickness Reynolds number and compare it with the critical momentum thickness Reynolds number. However, the models need to use an exhausting search algorithm to calculate the momentum thickness Reynolds number for complex flows. In other words, these models require high computational costs and complex coding requirements in CFD analyses. As a result, they are not practical in CFD simulations for various flows and complex geometries. The Dhawan and Narasimha model [15] is the first attempt at correlation-based transition models. They proposed an algebraic intermittency function, such as:

$$\gamma = \begin{cases} 0, & x < x_t \\ 1.0 - exp\left[-\frac{(x-x_t)^2 n\sigma}{U}\right] = 1.0 - exp(-0.41\xi^2) & x \geq x_t \end{cases} \tag{1.3}$$

The model assumes transition onset, x_t, is known as apriori since it is needed for the solution of the algebraic intermittency equation. The laminar and turbulent regions can be combined by solving the above equation.

Steelant and Dick [20] proposed a transport equation called conditional Navier- Stokes equations.

$$\frac{\partial \gamma}{\partial t} + \frac{\partial \rho u \gamma}{\partial x} + \frac{\partial \rho v \gamma}{\partial y} = (1-\gamma)\rho\sqrt{u^2+v^2}\beta(s) \tag{1.4}$$

The transport equation is derived from the intermittency function proposed by Dhawan and Narasimha [15]. The model can predict intermittency in the streamwise direction by assuming uniform intermittency distribution in the cross-stream direction. However, their approach is not consistent with experimental data.

Cho and Chung [21] proposed a new transport equation coupled with the k-epsilon turbulence model.

$$u\frac{\partial\gamma}{\partial x_j} = D_\gamma + S_\gamma \tag{1.5}$$

The model itself cannot predict the onset of transition. However, intermittency profiles agree with the experimental results for various flow conditions.

Suzen and Huang [17] improved the intermittency equation approach significantly. There is a transport equation solved in this model, similarly. The intermittency transport equation includes source terms from the Steelant and Dick model and Cho and Chung model. The transport equation is coupled with Menter's shear stress transport turbulence model [22]. The superiority of the model is that the intermittency profile along the cross-stream direction can be predicted, which was the shortcoming of the previous models.

1.3.2 Models Depending on Nonlocal Flow Variables

These models use constants derived from observations and experiments in transport equations. A prominent feature of these models is that they are compatible with modern CFD codes as vorticity Reynolds Number is used. Re_V is calculated as follows;

$$Re_V = \frac{\rho y^2}{\mu}\Omega \tag{1.6}$$

In equation 1.6, y denotes the distance from the nearest wall. Since all variables used to calculate Re_V are local, Re_V is also a local variable that can be computed easily in CFD codes. Observations show that the local vorticity Reynolds Number, Re_V, is proportional to the momentum thickness Reynolds Number, Re_θ . Using the proportionality between the Re_V and Re_θ , Re_θ can be computed easily without solving the integral formulation. Furthermore, this relationship is valid for a wide range of flow types. Thus, local correlation transition models can be used to model transition in CFD simulations.

The first of these models proposed by Langtry and Menter is the $\gamma-(Re_{\theta t})$ model [4]. Two additional scalar transport equations are solved besides the SST model transport equations.

$$\frac{\partial(\rho\gamma)}{\partial t} + \frac{\partial(\rho u_j \gamma)}{\partial x_j} = P_\gamma - E_\gamma + \frac{\partial}{\partial x_j}\left[\left(\mu + \frac{\mu_t}{\sigma_f}\right)\frac{\partial \gamma}{\partial x_j}\right] \tag{1.7}$$

$$\frac{\partial(\rho \hat{Re}_{\theta t})}{\partial t} + \frac{\partial(\rho u_j \hat{Re}_{\theta t})}{\partial x_j} = P_{\theta t} + \frac{\partial}{\partial x_j}\left[\sigma_{\theta t}\left(\mu + \mu_t\right)\frac{\partial Re_{\theta t}}{\partial x_j}\right] \tag{1.8}$$

One equation is solved for intermittency, another for transition momentum thickness Reynolds Number ($Re_{\theta t}$). Transport equations consist of local variables. Therefore, the $\gamma - (Re_{\theta t})$ model can be used for complex flows with any grid type. For these reasons, it is the most widely used transition model in CFD calculations [16].

After the success of the $\gamma - (Re_{\theta t})$ model, Menter proposed the simplified version of the $\gamma - (Re_{\theta t})$ model [5]. In the new model, called Menter's one equation γ model, the $(Re_{\theta t})$ transport equation is removed, and experimental correlations are embedded into the intermittency equation. The transport equation is the same as the $\gamma - (Re_{\theta t})$ model transport equation; however, source terms are slightly modified, and some constants are different.

$$\frac{\partial(\rho\gamma)}{\partial t} + \frac{\partial(\rho u_j \gamma)}{\partial x_j} = P_\gamma - E_\gamma + \frac{\partial}{\partial x_j}\left[\left(\mu + \frac{\mu_t}{\sigma_f}\right)\frac{\partial \gamma}{\partial x_j}\right] \tag{1.9}$$

Although one of the equations is removed, the new model gives acceptable predictions. The main advantage of the γ model is that it solves one less equation than the $\gamma - (Re_{\theta t})$ model. As a result, the new model is computationally cheaper. Furthermore, Galilean invariance is maintained in the latter model [5], which means problems with moving walls can also be solved with the γ model.

Another local correlation-based transition model is the Walters-Cokljat $k_T - k_L - \omega$ model [18]. This model is based on the concept that the cause of the bypass transition is very high amplitude streamwise fluctuations. These fluctuations are different from turbulent fluctuations, and they can be distinguished. Mayle and Schulz proposed a second kinetic energy equation to describe these fluctuations [13]. This kinetic energy was called laminar kinetic energy k_L. In this model, total kinetic energy is assumed to be the sum of the energy of large-scale eddies and small-scale eddies. Large-scale eddies contribute to laminar kinetic energy, and small-scale eddies contribute to tur-

bulent kinetic energy production. Thus, the transition can be modeled by calculating the k_L. Besides the merely changed $k-\omega$ transport equations, one more transport equation is solved to calculate laminar kinetic energy.

$$\frac{Dk_L}{Dt} = P_{k_L} - R_{BP} - R_{NAT} - D_L + \frac{\partial}{\partial x_j}\left[\nu \frac{\partial k_L}{\partial x_j}\right] \tag{1.10}$$

Since this model uses local formulation, it can be used in CFD codes.

The last model mentioned is Bas-Cakmakcioglu (BCM) algebraic transition model [19]. This model solves one algebraic equation instead of a partial differential equation for intermittency. The main idea of this model is to introduce a correlation-based intermittency function without a new transport equation, hence reducing the computational cost of CFD simulations. BCM model damps the turbulent production term until the threshold production value. After reaching this point, damping is reduced, and flow is considered fully turbulent. The intermittency equation is multiplied by the production term of the Spalart-Allmaras (S-A) turbulence model, and the transition is controlled accordingly. Lately, the model has become Galilean invariant with modification on the formulation [23]. Thus, the BCM algebraic transition model can be used for a wide range of flows with any type of grid.

1.3.3 Direct Numerical Simulation and Large Eddy Simulation

Using the DNS method, simulation of turbulent to laminar flow can be done most accurately. In this method, opposite to transition models previously mentioned, unsteady Navier Stokes equations are solved directly. Since Reynolds averaging is not used, there is no need to use a closure transition model. However, this method requires an extremely fine grid and, as a result, a very small-time step. Due to these reasons, this method is not practical in industrial applications. However, a limited number of DNS analyses are performed to produce some benchmark cases aimed at validation of the developed transition models [7, 16].

In the LES method, eddies are filtered according to their sizes first. Eddies with a size larger than a threshold are treated the same as in the DNS method, whereas smaller

eddies are modeled with a subgrid model. Thus, LES is faster than DNS. However, LES simulations are still expensive for routine industrial applications as substantial computational power is required. Instead, similar to the DNS method, this method is used to validate the other models being developed [7, 16].

1.4 Objectives

The transition is becoming important, and transition models are added to CFD codes. ANSYS software provides the $\gamma - (Re_{\theta t})$ transition model as Menter's model gains popularity. Bas-Cakmacioglu transition model is another prominent model added to open-source CFD code SU^2 in recent years. [5, 16, 19].

The objective of the thesis is to implement the Menter one-equation γ model in the in-house open-source-based CFD code and observe the performance of the model for different geometries with different flow conditions. Using the Menter one-equation γ model in real-life applications can be tricky for several reasons that will be explained in the discussions. Our solver already has Bas-Cakmacioglu zero-equation transition models. Well-known benchmark test cases were solved using the transition models, and the results were compared with the experimental data. Also, the advantages and disadvantages of the models were explained. The objective of the thesis is to make a clear assessment of mentioned transition models and assess some standard benchmark test cases.

1.5 Scope of Thesis

This study involves the implementation of the Menter one-equation γ model on our CFD solver. An assessment of the model was done using the experimental data. In, the implemented model is compared with available transition models. A mesh independence study is performed using different mesh sizes to provide meshing guidelines for transition problems. The assessment of the model is done using the experimental data of zero pressure gradient flat plate cases, Schubauer&Klebanoff, T3A, T3B, T3A- and non-zero pressure gradient flat plate cases, T3C2, T3C3, T3C4, T3C5. In

addition to flat plate cases, 2D airfoil cases are also investigated. Skin friction coefficient results and pressure distributions are compared to available experimental data. The advantages and disadvantages of the model are explained in the conclusion chapter. Future works are also pointed out.

CHAPTER 2

METHODOLOGY

In this thesis, Menter's one equation γ model [5] is implemented and assessed by comparing it with other transition models. This section describes the implemented transition model in detail. Secondly, the mesh domain used in simulations is also elaborated on in this section.

2.1 Transition Prediction

A transition model should predict the onset and length of the transition. These are the two essential features of a transition model. In this section, important concepts used in the Menter one-equation γ model to model transition accurately will be emphasized. Transition length and characteristics are controlled by intermittency. Transition onset is predicted by correlations based on experiments.

2.1.1 Intermittency

Intermittency refers to the probability of a point being in the turbulent region or not. It was mentioned that transition occurs through the formation of turbulent spots in the boundary layer. Emmons proposed the mathematical description of intermittency as a probabilistic function of space and time [24].

If a random point is chosen in the fully turbulent boundary, intermittency equals one. If the flow is laminar, the intermittency is zero. Based on this definition, various models with mathematical descriptions of intermittency developed.

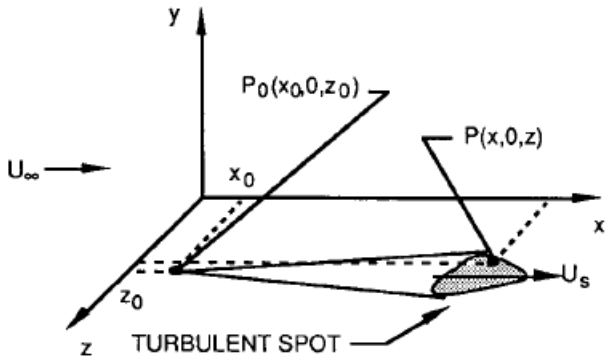

Figure 2.1: Intermittency in Space [7]

Intermittency can be modeled with an algebraic function or with a transport equation. Earlier models of intermittency were in algebraic form. Over time, transport equations are proposed for intermittency. Source terms of the transport equations are responsible for the algebraic transition models in these equations. Modeling intermittency with the transport equation provides the modeling transition both across the boundary layer and in the streamwise direction [7]. Thus, this approach gives more accurate solutions than the algebraic approaches.

The task of intermittency is to control the transition characteristics and length of the transition [16, 7]. As the boundary layer develops, intermittency, γ, increases and eventually, γ becomes equal to unity [24]. From this point on, the transition phase is completed, and the flow becomes fully turbulent. The underlying turbulence model is employed for turbulent flow. However, another mechanism besides the intermittency is required to predict the onset of the transition.

2.1.2 Prediction of Transition Onset

Momentum thickness is the distance from which the surface must be displaced such that, with no boundary layer, the total flow momentum is conserved.

$$\delta_2 = \int_0^\infty \frac{\rho u}{u_\infty \rho_\infty} \left(1 - \frac{u}{u_\infty}\right) dy \tag{2.1}$$

Momentum thickness Reynolds number is a flow parameter that is calculated using the momentum thickness

$$Re_\theta = \frac{\rho U_\infty \delta_2}{\mu} \tag{2.2}$$

Transition onset momentum thickness Reynolds number, $Re_{\theta t}$, is the momentum thickness Reynolds number calculated at transition onset.

Studies and experiments show that transition onset is strongly related to turbulence intensity and pressure gradient[4, 11, 1]. Turbulence intensity, also often referred to as turbulence level, is a measure of the strength of velocity fluctuations in a turbulent flow field. Experiments have shown that transition onset is earlier as turbulent intensity increases. In other words, as freestream turbulent intensity grows, transition onset momentum thickness Reynolds Number, $Re_{\theta t}$, gets smaller.

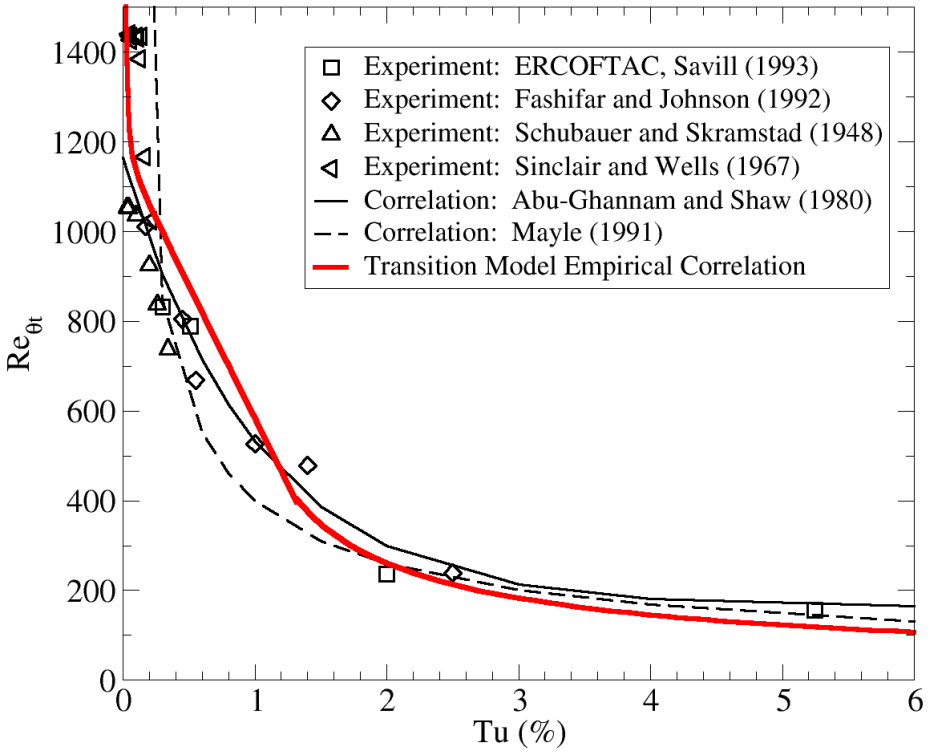

Figure 2.2: Relation between the Turbulence Intensity and Transition Onset Momentum Thickness Reynolds Number [11]

Thus, a transition model should include the effect of turbulence intensity. Menter's one-equation γ model multiplies the source term of the intermittency transport equation with a term including turbulence intensity [5].

The pressure gradient is decisive for the transition onset, similar to turbulence inten-

sity. As shown in 2.2, the transition onset momentum thickness Reynolds number decreases with increasing turbulence intensity. In other words, transition onset delays with a larger pressure gradient in the boundary layer [8].

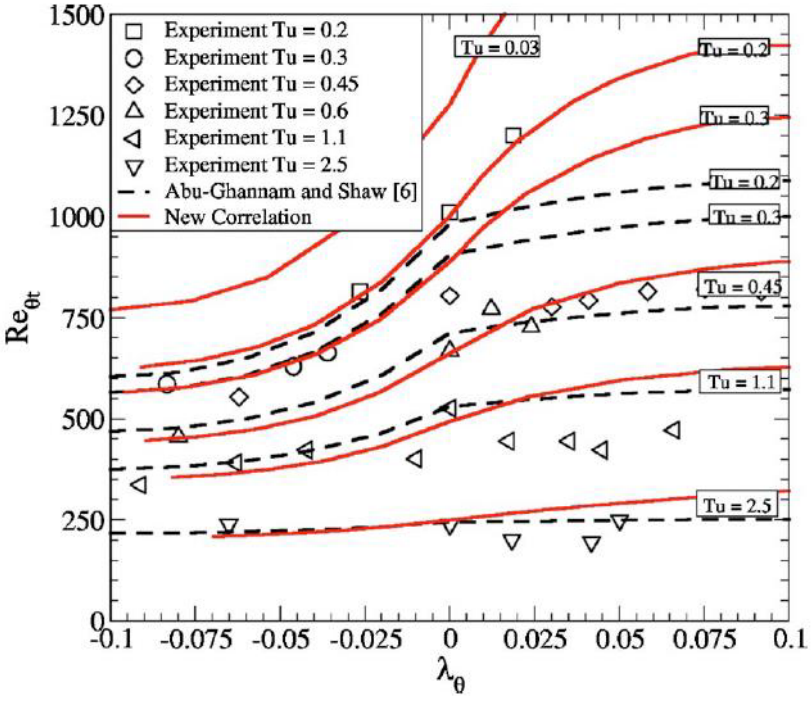

Figure 2.3: Relation between the Pressure Gradient Parameter and Transition Onset Momentum Thickness Reynolds Number [11]

To include the effect of the pressure gradient, the pressure gradient parameter term, λ_θ, is added to the multiplying term of the production term in the intermittency transport equation, besides the turbulent intensity.

2.2 Menter One-Equation γ Model

Menter's one-equation γ model is a simplified version of the $\gamma - (Re_{\theta t})$ model. It solves one additional transport equation besides the transport equations of the underlying turbulence model in a similar fashion as the $\gamma - (Re_{\theta t})$ model does. The difference between one equation γ model from the $\gamma - (Re_{\theta t})$ model is that the former does not solve any transport equation for momentum thickness Reynolds number, $(Re_{\theta t})$.

Instead, $(Re_{\theta t})$ is computed algebraically using local variables in the transport equation for intermittency. Thus, the new model becomes Galilean invariant. In other words, the one-equation γ model can be used for moving walls opposite the $\gamma-(Re_{\theta t})$ model.

The underlying turbulence model of the Menter's one equation γ model is $k-\omega$ SST [22]. The importance of the underlying turbulence model is that it should have a proper viscous sublayer formulation. Therefore, laminar and transitional flow can be resolved to represent the physics of the transition. The intermittency transport equation is coupled with the SST turbulence model as the $k-\omega$ SST model can capture the viscous sublayer. However, transport equations of the underlying turbulence model are slightly modified in the one-equation γ model. The reason behind this modification is to control the production term of turbulent kinetic energy in the transition phase.

Menter one equation γ model is calibrated with available experimental data. Calibration for all types of flows would result in a complex model, which is undesirable. Instead, calibration is done for self-similar flows, steady two- dimensional laminar flow around the wedge (Falkner-Skan family). Non-equilibrium flows, mainly with separation, are also considered during calibration [5]. The adjustment of the model coefficients according to self-similar flows and separation results in some differences with experimental data for different transition mechanisms. In other words, it would not surprise to predict the wake-induced transition with error since this type of mechanism is not included in the calibration of coefficients.

The novelty of the Menter one-equation γ model is that, unlike turbulence models, this model does not seek to represent the physics of the transition process but rather provides a framework for incorporating correlation-based models into general-purpose CFD codes. The physics of the transition phenomenon is contained in the model's empirical correlations. As a result, this formulation is not confined to a single transition mechanism, such as natural transition or bypass transition. The formulation can be applied to any transition mode as long as modifications of the correlations are embedded into the model coefficients [5].

The advantages of the one equation γ model over the $\gamma-(Re_{\theta t})$ model are as follows

[5]:

- One equation γ model solves less number of partial differential equations, which makes the model computationally cheaper,
- One equation γ model is Galilean invariant, whereas the $\gamma - (Re_{\theta t})$ model is not,
- It is much simpler than the $\gamma - (Re_{\theta t})$ model, which results in fine-tuning the new model is simpler than fine-tuning the $\gamma - (Re_{\theta t})$ model. In other words, since the new model has fewer equations than the former one, fine-tuning is easier.

A transition model should predict the onset and length of the transition. These are the two essential features of a transition model. Menter one equation γ model handles triggering the transition with accurate transition length using the intermittency concept. Transition onset is predicted using the experimental correlations that relate the turbulence intensity and pressure gradient to the transition phenomenon.

2.2.1 Transport Equations of Transition Model

The intermittency transport equation of the Menter one equation γ model is presented below.

$$\frac{\partial(\rho\gamma)}{\partial t} + \frac{\partial(\rho U_j \gamma)}{\partial x_j} = P_\gamma - E_\gamma + \frac{\partial}{\partial x_j}\left[\left(\mu + \frac{\mu_t}{\sigma_f}\right)\frac{\partial \gamma}{\partial x_j}\right] \tag{2.3}$$

The γ production term is defined as:

$$P_\gamma = F_{length}\rho S\gamma(1-\gamma)F_{onset} \tag{2.4}$$

In equation 2.4, S refers to the strain rate magnitude. It is included in the production term as a multiplier as strain rate is the driving factor of the transition process. F_{length} is a calibration constant. F_{onset} is the term that triggers the onset of the transition.

This term involves the ratio of vorticity Reynolds number to critical Reynolds number, between which a strong relationship is shown experimentally [5].

Before the onset of the transition, where flow is laminar, the production term is equal to zero, as expected.

The destruction term in the transport equation is as follows:

$$E_\gamma = c_{a2}\rho\Omega\gamma F_{turb}(c_{e2}\gamma - 1) \tag{2.5}$$

Constants used in the production and destruction terms are given below.

$F_{length} = 100$,$c_{e2} = 50$,$c_{a2} = 0.06$,$\sigma_\gamma = 1.0$,

Functions used in calculating the production and destruction terms are given below.

$F_{onset1} = \frac{Re_V}{2.2Re_{\theta c}}$,$F_{onset2} = min(F_{onset1}, 2.0)$,

$F_{onset3} = max\left(1 - \left[\frac{R_T}{3.5}\right]^3, 0\right)$,$F_{onset} = max(F_{onset2} - F_{onset3}, 0)$,

$F_{turb} = e^{-\left(\frac{R_T}{4}\right)^2}$,$R_T = \frac{\rho k}{\mu\omega}$, $Re_V = \frac{\rho d_\omega^2 S}{\mu}$,$Re_{\theta c} = f(Tu_L, \lambda_{\theta L}$

k and ω in the formulations refer to the turbulent kinetic energy and turbulence frequency calculated from the transport equation of the underlying turbulence model, SST. The term d_ω refers to the wall distance.

The boundary conditions of the transport γ-model are that flux of the γ through the wall is zero, and γ equals unity at the inlet to preserve the freestream turbulence decay rate of the underlying turbulence model [4].

The critical momentum thickness Reynolds number, $Re_{\theta c}$, is defined as a function of the local turbulent intensity and local pressure gradient parameter. Thus, to calculate $Re_{\theta c}$, local turbulent intensity and local pressure gradient parameters are calculated. Local turbulent intensity, Tu_L, is defined as:

$$Tu_L = min\left(100\frac{\sqrt{2k/3}}{\omega d_\omega}, 100\right) \tag{2.6}$$

This formulation allows that local turbulent intensity is equal to the freestream turbulent intensity in the middle of the boundary layer. The pressure gradient parameter is defined as follows:

$$\lambda_{\theta L} = -7.57x10^{-3}\frac{dV}{dy}\frac{d_\omega^2}{\nu} + 0.0128 \tag{2.7}$$

Coefficients in this formula are selected considering the self-similar flows. To achieve numerical robustness, Menter bounded $\lambda_{\theta L}$ as follows:

$$\lambda_{\theta L} = min(max(\lambda_{\theta L}, -1.0), 1.0) \tag{2.8}$$

2.2.2 Coupling with SST Turbulence Model

The coupling of the Menter one equation γ model with the SST turbulence model is done by slightly modifying the transport original transport equations of turbulent kinetic energy [5].

$$\frac{\partial}{\partial t}(\rho k) + \frac{\partial}{\partial x_j}(\rho u_j k) = \tilde{P}_k + P_k^{lim} - \tilde{D}_k + \frac{\partial}{\partial x_j}\left[(\mu + \sigma_k \mu_t)\frac{\partial k}{\partial x_j}\right] \tag{2.9}$$

$$\frac{\partial}{\partial t}(\rho \omega) + \frac{\partial}{\partial x_j}(\rho u_j \omega) = \alpha\frac{P_k}{\nu_t} - D_\omega + CD_\omega + \frac{\partial}{\partial x_j}\left[(\mu + \sigma_\omega \mu_t)\frac{\partial \omega}{\partial x_j}\right] \tag{2.10}$$

$$\tilde{P}_\gamma = \gamma P_k \tag{2.11}$$

$$\tilde{D}_\gamma = max(\gamma, 0.1)D_k \tag{2.12}$$

Where P_k and D_k are the production and destruction terms of the original turbulent kinetic energy of the equation of SST. The updated k equation includes the term P_k^{lim} to provide the generation of k at the transition phase for small turbulence intensity

values. Without this term, it is observed that the underlying turbulence model can produce turbulence with delay.

$$P_k^{lim} = 5C_k max(\gamma - 0.2, 0)(1 - \gamma)F_{on}^{lim} max(3C_{sep}\mu - \mu_t, 0)S\Omega \tag{2.13}$$

$$F_{on}^{lim} = min(max\left(\frac{Re_V}{2.2Re_C^{lim}} - 1, 0\right), 3) \tag{2.14}$$

$Re_{\theta c}^{lim} = 1100$,$c_k = 1.0$,$c_{sep} = 1.0$

The term is only engaged if the transition model is engaged and the γ exceeds 0.2. When the flow becomes fully turbulent, the term P_k^{lim} is turned off. This term helps the transition model to be more reliable for low turbulence intensity and laminar separation flows.

2.3 CFD Solver

All developments are implemented in our cell-based finite volume solver. The solver is based on an open-source flow solver, flowpsi, which is built on the Loci Framework. The Loci Framework is a rule-based programming framework that involves auto parallelization, finite volume tools, and sparse matrix solvers.

The turbulence models in the solvers are built as runtime libraries. Various variants of Spalart-Allmaras, $k - \omega$ and $k_L - k_T - \omega$ (WalterColkjat) turbulence models are available in the solver.

The current $k-\omega-\gamma$ development is applied as a new turbulent solver library starting from the $k - \omega$ model. All the necessary modifications are done, and changes to the SST model are implemented. The Baş-Çakmakçıoğlu model, however, is added directly to the SA solver. The implementation of the Baş Çakmakçıoğlu transition model is highly straightforward. The user may turn the transition on with a flag in the run-file with the new implementation.

All the runs are performed using the HLLC flux solver for inviscid fluxes. HLLC is

an approximate Riemann solver, and it is one of the outstanding methods for inviscid compressible flows. As with all Riemannian solvers, the original form of HLLC suffers from slow convergence at small Mach numbers. Our code employs preconditioning for this regime. In the thesis, we have carefully set the preconditioning parameters to ensure convergence.

The applied flux scheme is 2^{nd} order accurate HLLC with Venkatakrishnan limiter. The solver is implicit with a variable time step technique. All test cases are run with the same settings with the sole difference of preconditioning. The verifications show that both transition models exhibit very similar results to the reference papers. Minor differences may have resulted from the Riemannian (compressible) flux scheme, computational mesh difference or selection of flow domain in pressure-gradient cases.

2.4 Mesh Generation

Transitional simulations require good quality mesh since the viscous sublayer is resolved to predict the transition. To solve the laminar sublayer, sufficient numbers of cells are needed in the normal to wall direction. Furthermore, it is shown that the $\gamma - (Re_{\theta t})$and Menter one equation γ model is sensitive to mesh properties both streamwise and normal to wall directions [5, 8]. Menter et al. (2015) recommend following practice rules in mesh generation for Menter one equation γ model;

- Dimensionless wall distance $y+$ value should be less than one,
- The expansion ratio in the normal wall direction should be less than 1.1,
- At least 30 cells normal to wall direction,
- At least 100 cells in a streamwise direction.

The grid convergence studies for all cases are conducted, and one study is presented for the Schubauer-Klebanoff case. Five different meshes with different numbers of cells are created considering the guidelines mentioned above. Properties of the grids are given in table 2.1.

Table 2.1: Meshes used in grid convergence study

Mesh ID	Stream-wise node numbers	Normal to wall node numbers
$M1$	120	80
$M2$	160	120
$M3$	240	160
$M4$	360	240
$M5$	480	320

The drag convergence plot is given in figure 2.4. The x-axis represents the $(1/N)^{1/2}$, which is proportional to average grid spacing, h. Very left of the plot, $h = 0$, represents the infinitely fine grid. The solution converges with the smaller mesh size.

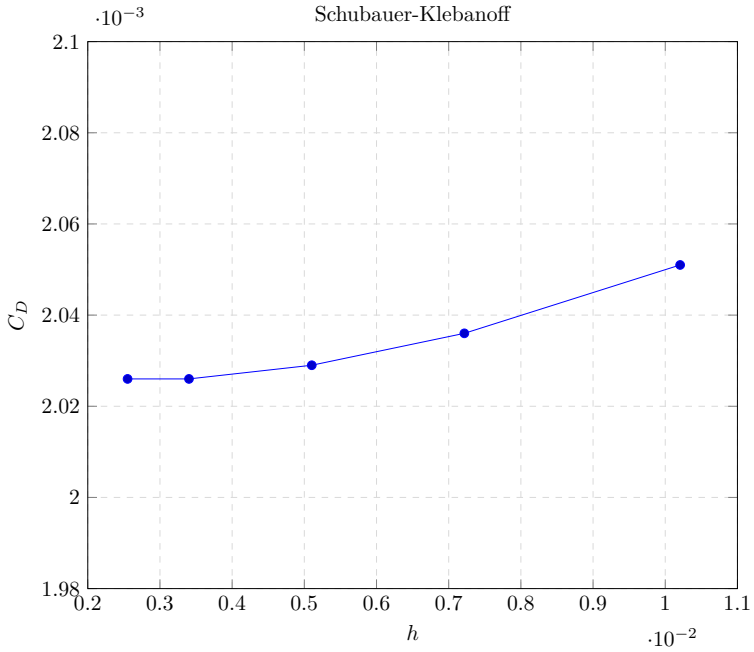

Figure 2.4: Drag Convergence

Skin friction coefficients obtained using five grids are reported in figure 2.5.

Similar to the drag coefficient, skin friction coefficients converge as the element size in the streamwise direction decreases. Considering our computational resources, Mesh 3 is selected, and the rest of the study is conducted using the selected mesh domain for the SK case. For other test cases, a similar approach was applied. The mesh independence studies of the other cases are not involved in this thesis.

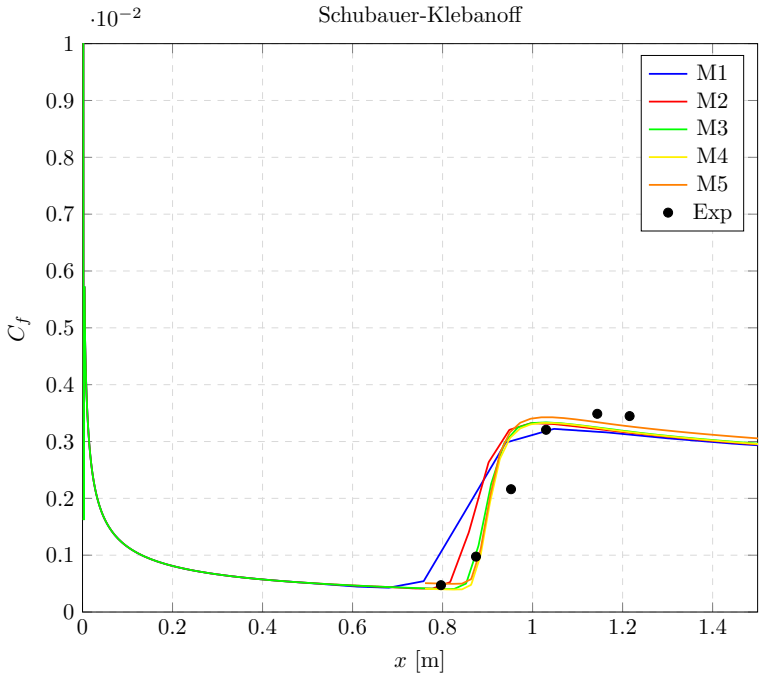

Figure 2.5: Skin friction coefficients obtained using five meshes

Properties of meshes used are presented in Table 2.2

Table 2.2: Meshes Properties

Case	Cells	Expansion Ratio	First Cell Thickness	y+
Zero Pressure Gradient	$240 \times 160 \times 1$	1.08	$2x10^{-5}$	0.8
Nonzero Pressure Gradient	$255 \times 150 \times 1$	1.05	$1x10^{-5}$	0.7

2.5 Computational Domain

2.5.1 Zero Pressure Gradient Flat Plate Cases

Boundary conditions assigned to mesh obtained at the end of the mesh generation process are shown in figure 2.6.

At the inlet, velocity, pressure and density are specified with turbulent kinetic energy, k and dissipation rate, ω. The pressure outlet boundary condition is defined at the downstream boundary of the flow. The symmetry boundary condition is assigned to the surface between the flat plate and the inlet. The farfield boundary condition is

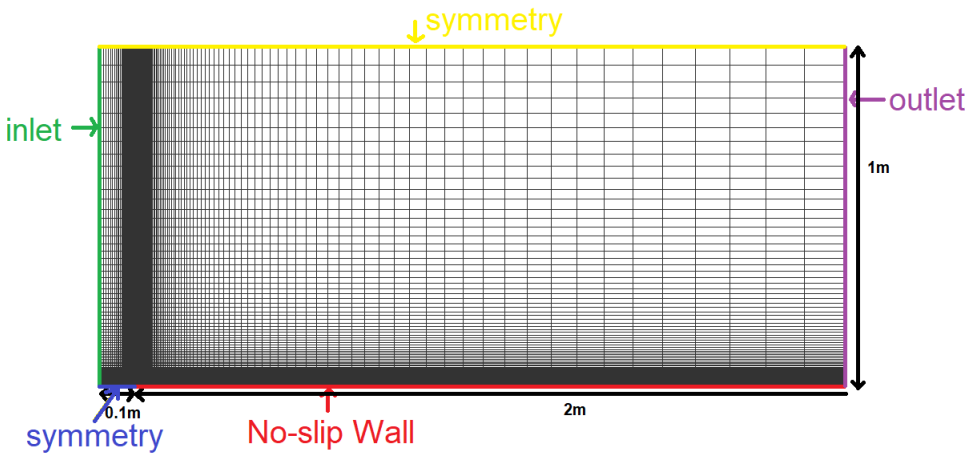

Figure 2.6: Computational Domain for Zero Pressure Gradient Cases

applied to the opposite of the wall. Very high-quality and dense mesh is defined at the leading edge of the flat plate. The reason for this is to resolve the stagnation point with reasonable accuracy. Cells parallel to the flat plate become coarser as the distance to the leading-edge increases. However, normal to the flat plate, cell distance is kept constant, and $y+$ is kept close to unity. The Klebanoff, T3A, T3B and T3A- test cases are solved using the mesh explained.

2.5.2 Flat Plate Cases with Pressure Gradient

T3C series are the cases with pressure gradients. The computational domain of T3C cases is generated in the converging-diverging duct form to simulate the pressure gradient.

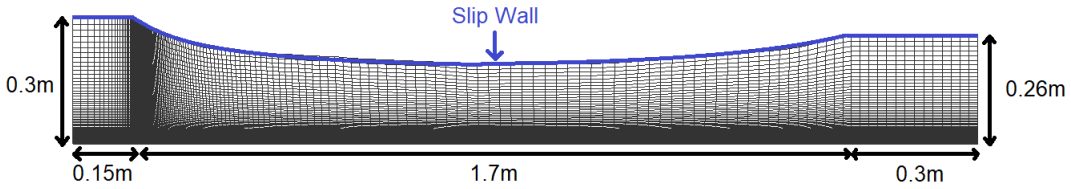

Figure 2.7: Mesh Domain for Cases with Pressure Gradient

Boundary conditions are assigned similar to mesh generated for zero pressure gradient cases. The only difference is that the slip wall is defined opposite the flat plate for the second mesh. The mesh density and the first layer thickness are specified with a similar approach with zero pressure gradient mesh.

CHAPTER 3

RESULTS & DISCUSSION

In this section, obtained results are given with experimental data, and comments are given.

3.1 Flat Plate Cases

Standard benchmark cases to test the development and implementation of transition models are available in the literature. The performance of the studied transition model is assessed, and validation studies are conducted by comparing the obtained results and experimental data. The Menter one-equation γ model is tested for different cases in several articles of Menter. Those are Schubauer-Klebanoff [25] and ERCOFTAC [26] series experiments.

The Schubauer-Klebanoff flat plate test case is one of the most well-known flat plate cases used to validate transition models. It was carried out in the 1950s and demonstrated a natural transition on a flat plate with low freestream turbulence intensity values [27].

The T3 experiments were conducted by Rolls Royce in the 1990s and have become benchmark cases for transition model validation [26]. The bypass transition mode dominates the transition in all T3 cases due to high freestream turbulence intensities. Freestream velocity profiles, freestream turbulence intensity profiles and skin friction coefficients are measured and reported in the T3 series. T3A, T3B and T3A- are zero pressure gradient flat plate cases. The effect of freestream velocity and freestream turbulence intensity are investigated in zero pressure gradient test cases. T3C series

are non-zero pressure gradients cases. The effect of pressure gradient with different freestream velocities and freestream turbulence intensities is studied in these cases.

In this thesis, velocities, turbulence intensities and viscosity ratios at the inlet are assigned according to experimental data to simulate each non-zero pressure gradient test case realistically. Test conditions are given in Table 3.1.

Table 3.1: Inlet Conditions of Different Test Cases

Case	$U_{in}[m/s]$	$Tu(\%)$	μ_t/μ	$\rho, kg/m^3$	$\mu, kg/ms$
S&K	50.1	0.18	1	1.2	1.8×10^{-5}
T3A	5.18	4.5	8	1.2	1.8×10^{-5}
T3B	9.4	7.8	80	1.2	1.8×10^{-5}
T3A-	19.8	1.1	6	1.2	1.8×10^{-5}
T3C2	5.4	3	9	1.2	1.8×10^{-5}
T3C3	4.0	3	5	1.2	1.8×10^{-5}
T3C4	1.4	3	2	1.2	1.8×10^{-5}
T3C5	9.1	7	12	1.2	1.8×10^{-5}

In addition to the Menter one-equation γ model, test cases are analyzed using the original SST and Bas-Cakmakcioglu models made available with a minor modification in our code. Results of all transition models are given in this section.

3.1.1 Schubauer-Klebanoff Test Case

Results of the Schubauer-Klebanoff test case show that Menter one equation γ model and the Bas-Cakmakcioglu model can predict natural transition accurately. Bas-Cakmakcioglu model predicts skin friction coefficient better than the Menter one-equation γ model after the flow becomes fully turbulent for the Schubauer-Klebanoff test case. Menter solution [5] is also given in figure 3.1. The turbulence decay is not reported for this experiment. The reason for the difference between his solution and our solution could be the difference in turbulence decay profiles.

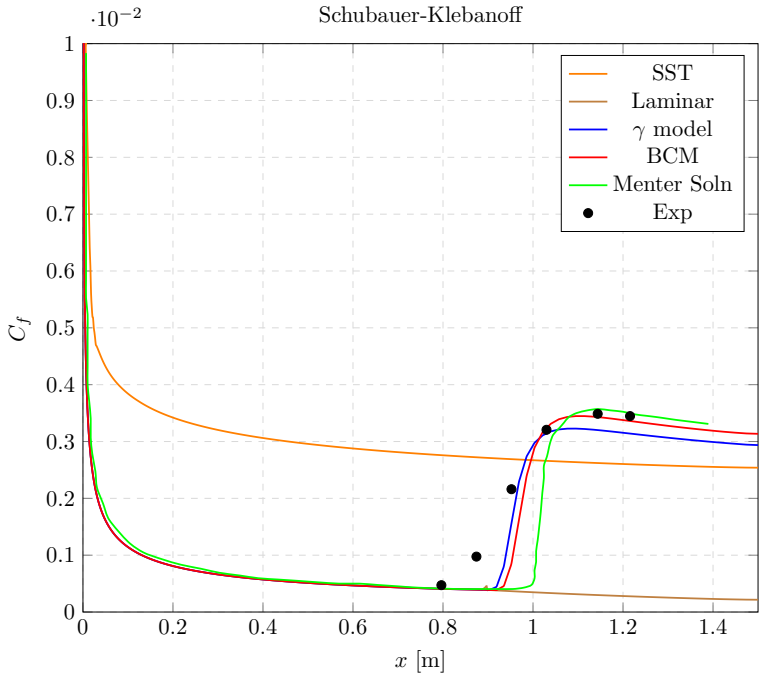

Figure 3.1: Comparison of Skin Friction Coefficients obtained with Different Models for S&K Case

3.1.2 Results for ERCOFTAC Zero Pressure Gradient Cases

T3A, T3B and T3A- zero pressure gradient cases are examined with the studied transition models. These cases are more challenging than the S&K case since they are bypass transition cases as turbulent intensities are larger than 1% or close to 1%. Thus, resolving transition in these cases is more challenging than in the S&K case. The inlet freestream turbulence intensity and viscosity ratio values are adjusted according to experimental turbulence intensity data. Turbulence intensity profiles and skin friction coefficients are given in the following figures.

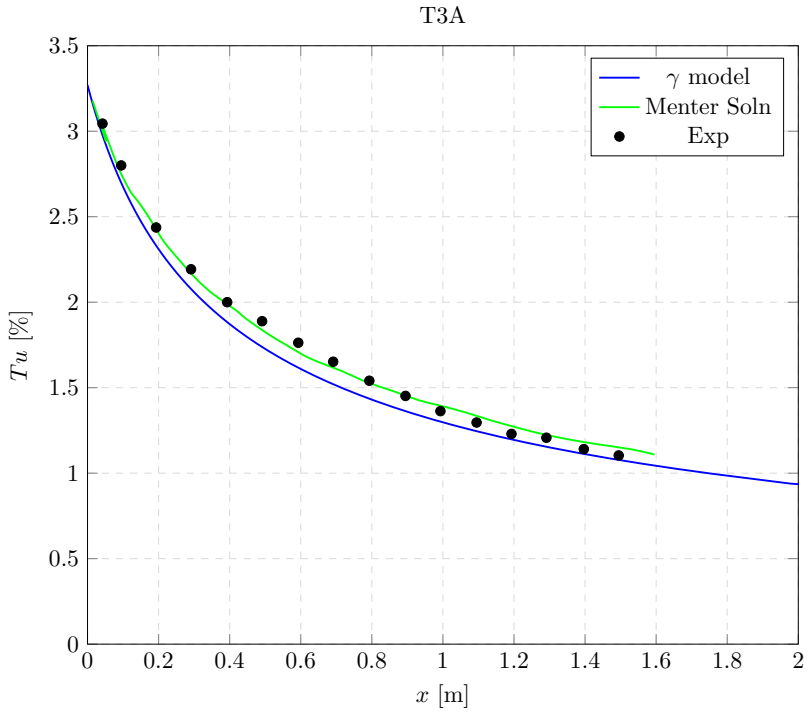

Figure 3.2: Turbulence intensity profile of T3A simulation

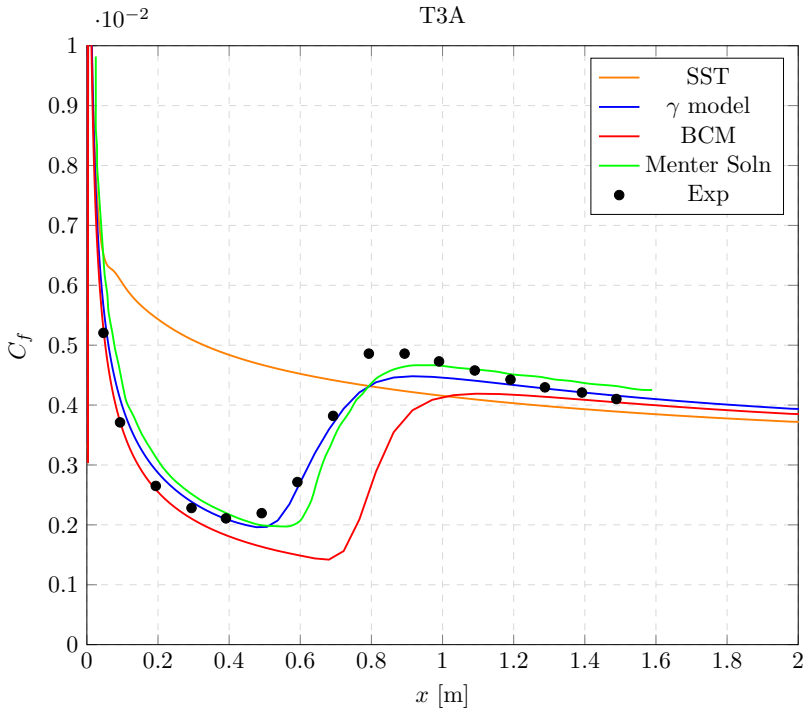

Figure 3.3: Comparison of Skin Friction Coefficients obtained with Different Models for T3A Case

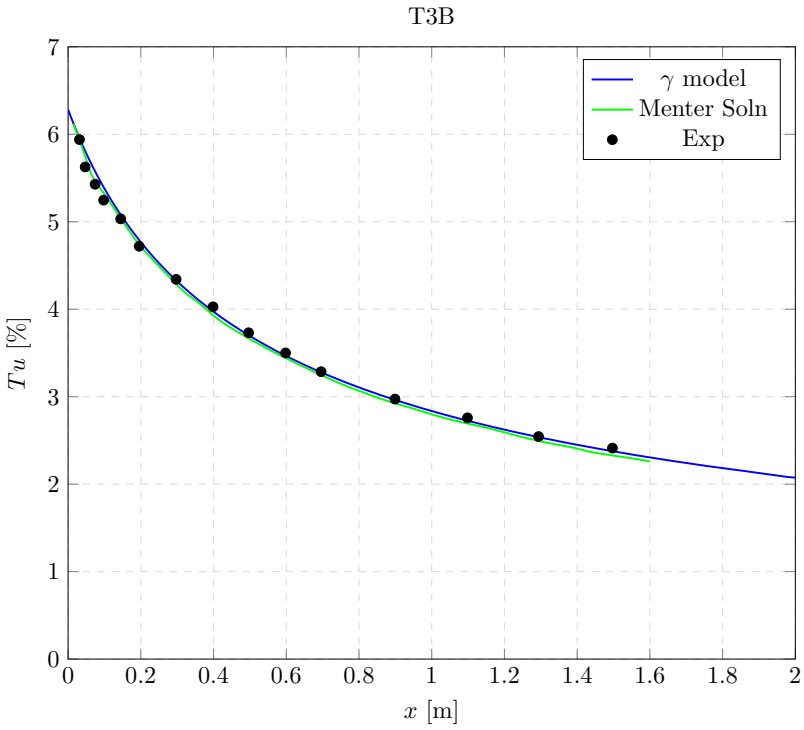

Figure 3.4: Turbulence intensity profile of T3B simulation

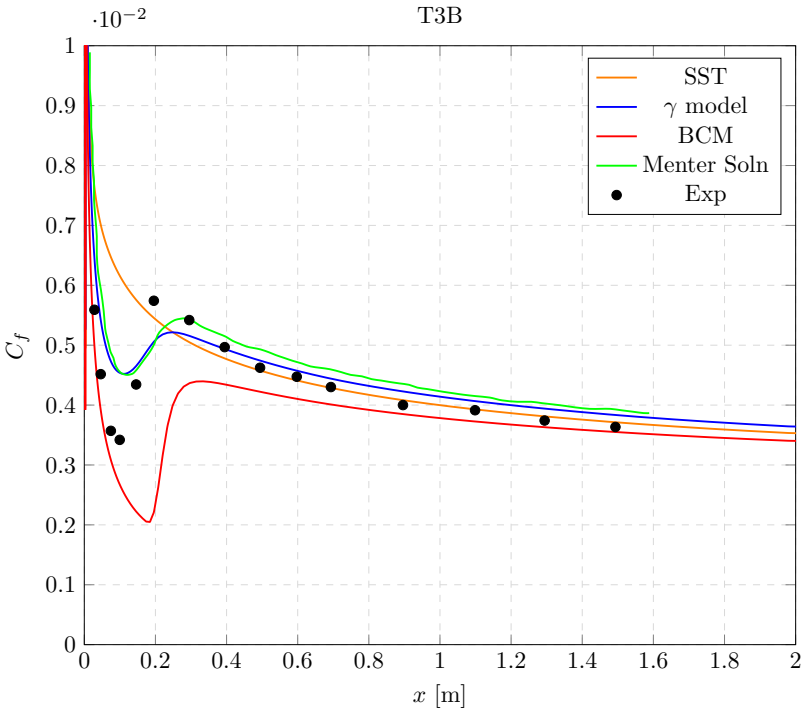

Figure 3.5: Comparison of Skin Friction Coefficients obtained with Different Models for T3B Case

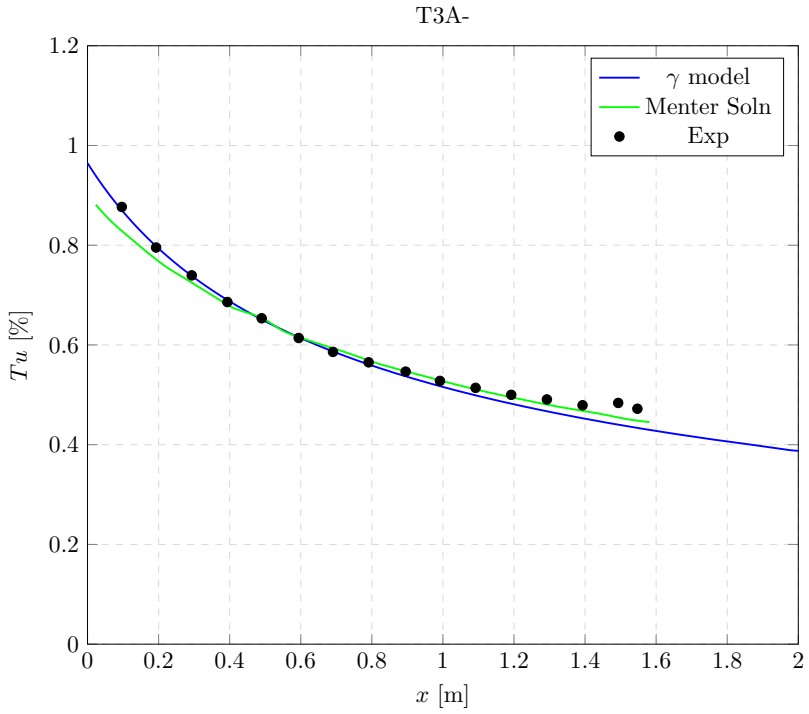

Figure 3.6: Turbulence intensity profile of T3A- simulation

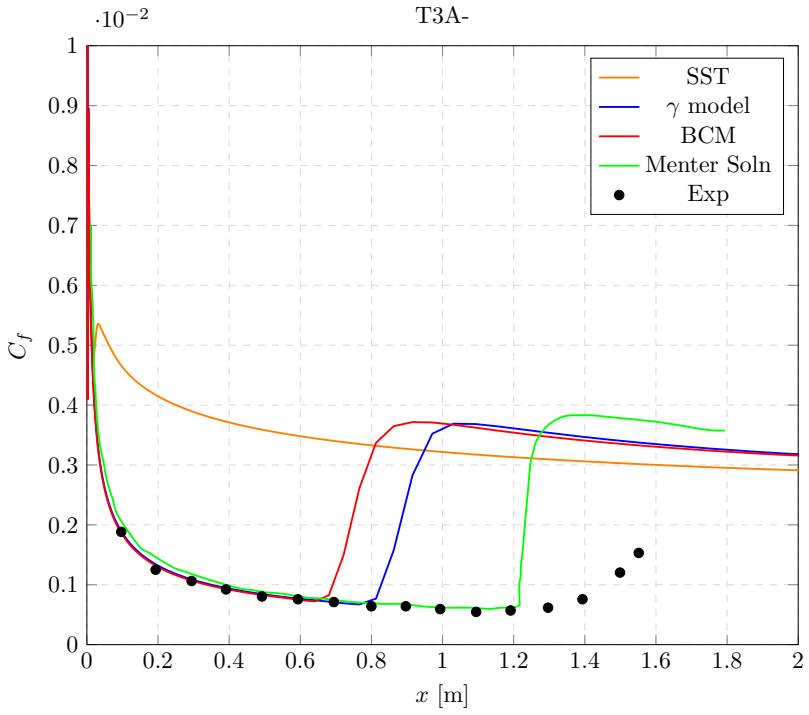

Figure 3.7: Comparison of Skin Friction Coefficients obtained with Different Models for T3A- Case

Menter's solutions are digitized from the original paper [5] and added to T3A and T3B plots to show that the model is implemented correctly. The small discrepancy between Menter's results and obtained results during this study could be the difference in flux schemes between the two codes. Nevertheless, the results match well.

Menter's one-equation γ model performed better than BCM for the T3A case. In the T3B case, the flow becomes fully turbulent immediately after interacting with the flat plate. The γ model and BCM have captured transition with reasonable accuracy. The challenging aspect of T3A- is that transition onset occurs at the end of the plate. None of the transition models could predict transition onset correctly.

3.1.3 Results for ERCOFTAC Non-Zero Pressure Gradient Cases

The ERCOFTAC test cases T3C2, T3C3, T3C4 and T3C5, are used to validate the model in the scenario of a transitional boundary layer with the influence of a pressure gradient. The favorable pressure gradients impact the transition onsets of T3C2, T3C3, T3C4 and T3C5 under various freestream velocity changes. Analyses are done using The Menter one-equation γ model and BCM. The results obtained in this section are highly dependent on computational domains. As mentioned previously, the pressure gradient is implemented using the converging-diverging duct shape domain. The upper boundary should be generated to satisfy the experimental data of local free stream flow velocity. The computational domain is obtained iteratively. The same domain is used for all T3C cases. Inlet turbulence intensity and viscosity ratios are assigned considering turbulence intensity profiles of experimental data. Velocity profiles obtained using the inlet conditions in table 3.1 are given in figures 3.8, 3.9, 3.10 and 3.11 for T3C cases.

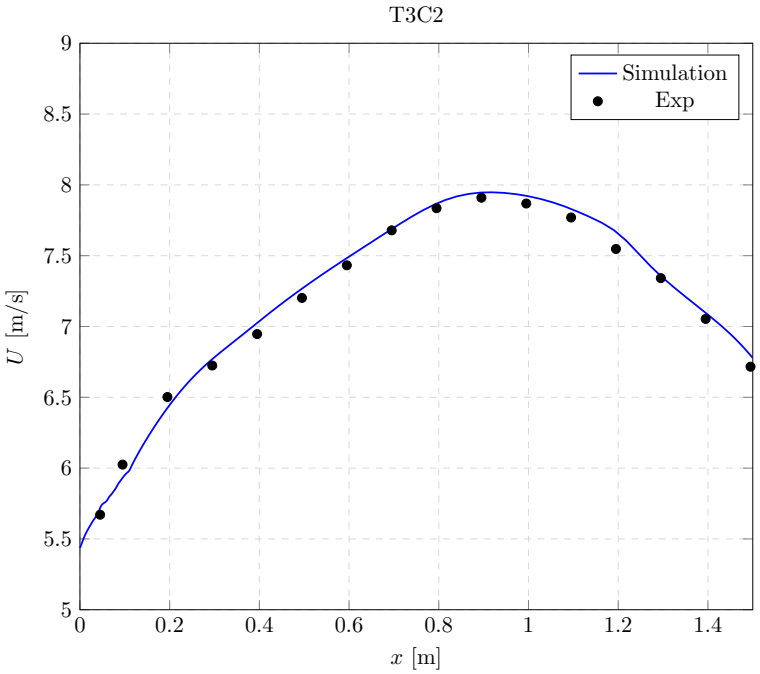

Figure 3.8: Distributions of freestream velocity for T3C2

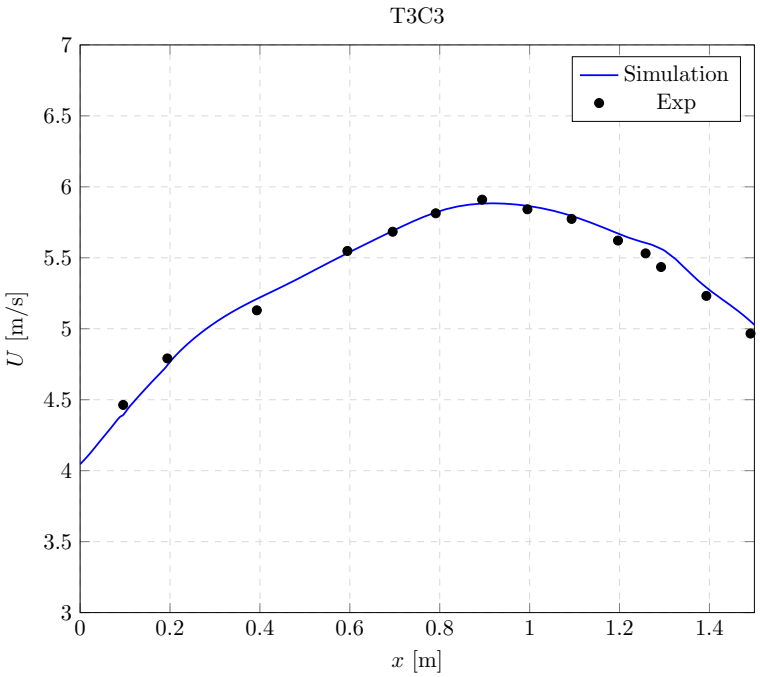

Figure 3.9: Distributions of freestream velocity for T3C3

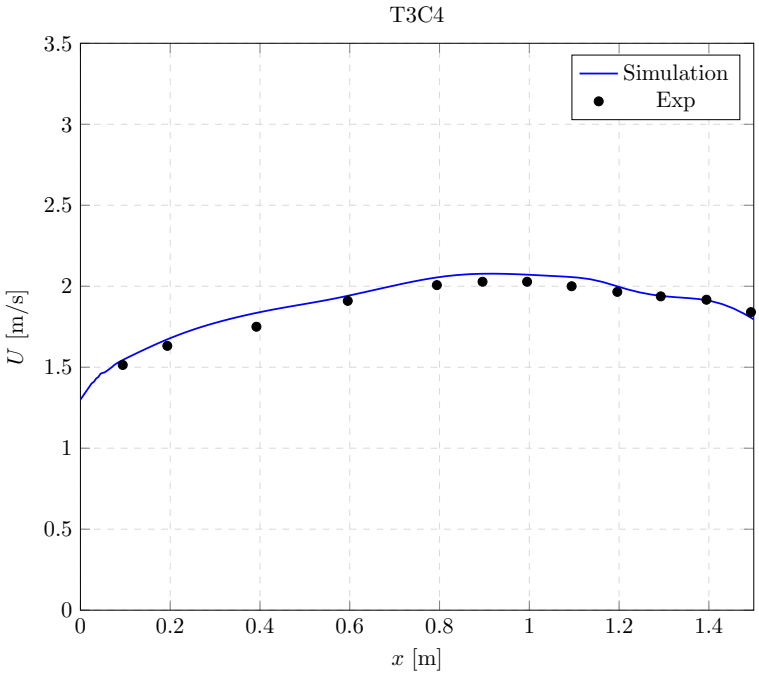

Figure 3.10: Distributions of freestream velocity for T3C4

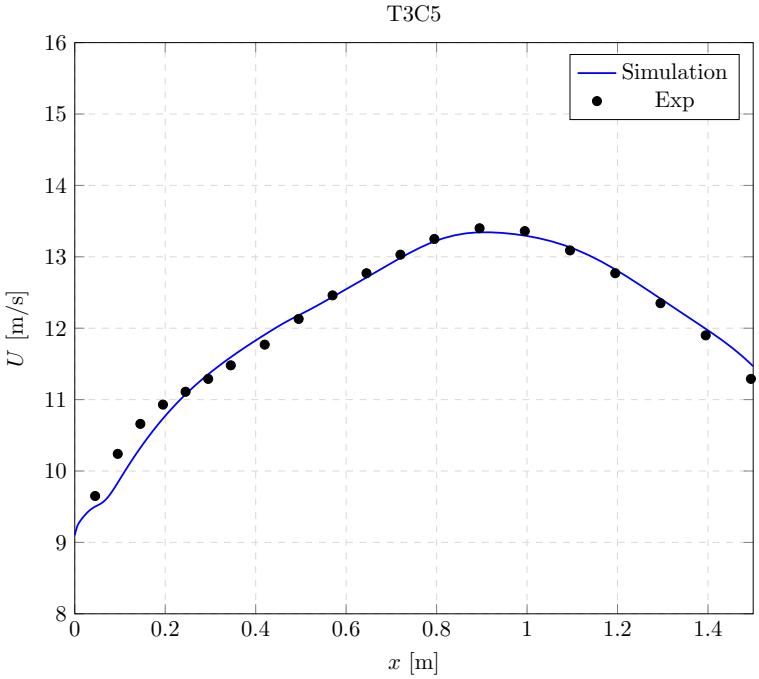

Figure 3.11: Distributions of freestream velocity for T3C5

Velocity profiles reasonably agree with the experimental data. Turbulence intensity profiles of the simulations are presented in the figures 3.12, 3.13, 3.14 and 3.15.

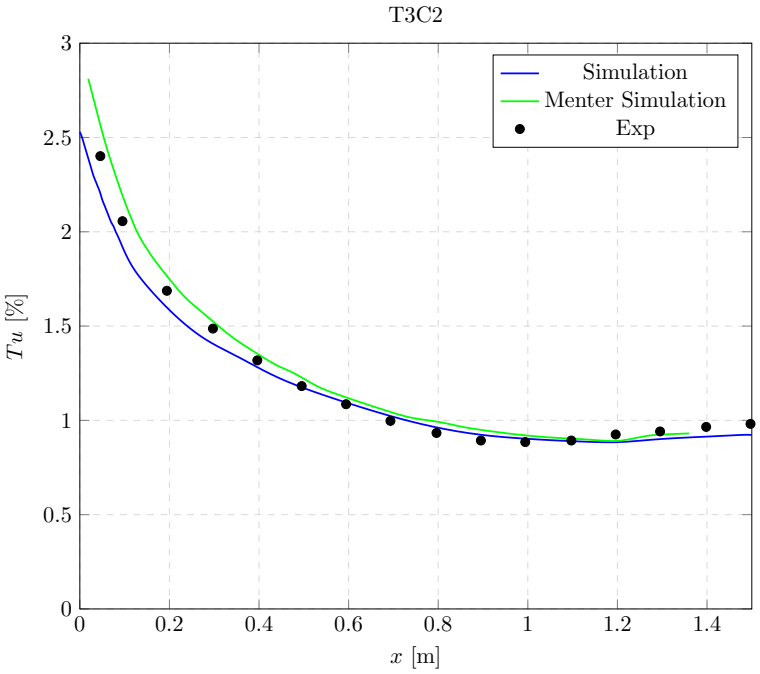

Figure 3.12: Turbulence intensity of T3C2 simulation

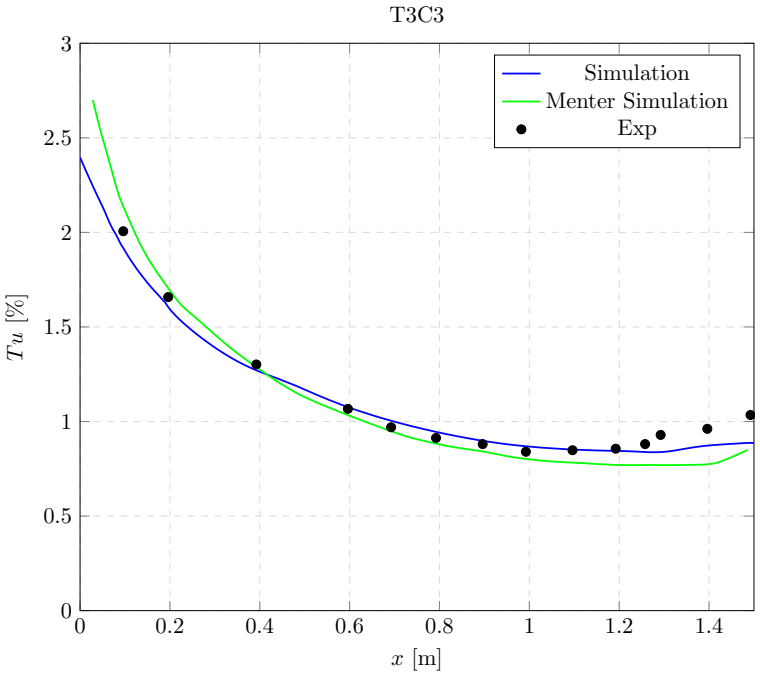

Figure 3.13: Turbulence intensity of T3C3 simulation

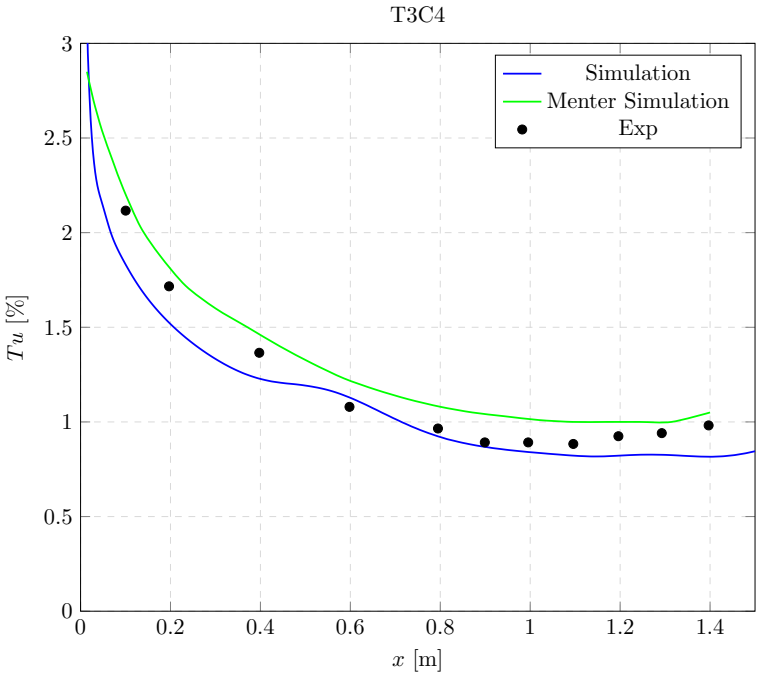

Figure 3.14: Turbulence intensity of T3C4 simulation

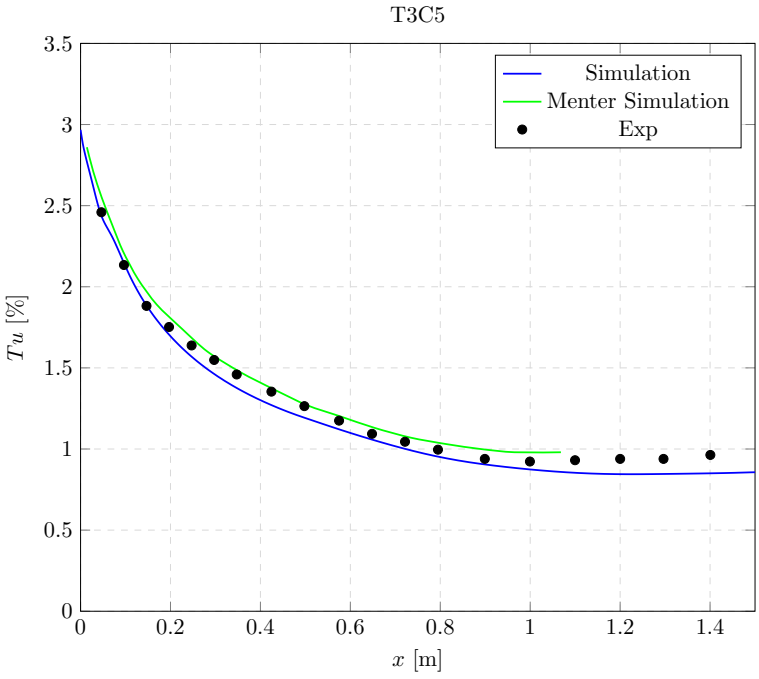

Figure 3.15: Turbulence intensity of T3C5 simulation

Turbulence intensity profiles of T3C cases seem to be quite good. Skin friction coefficients for T3C2, T3C3, T3C4 and T3C5 cases are presented in the figures 3.16,

3.17, 3.18 and 3.19.

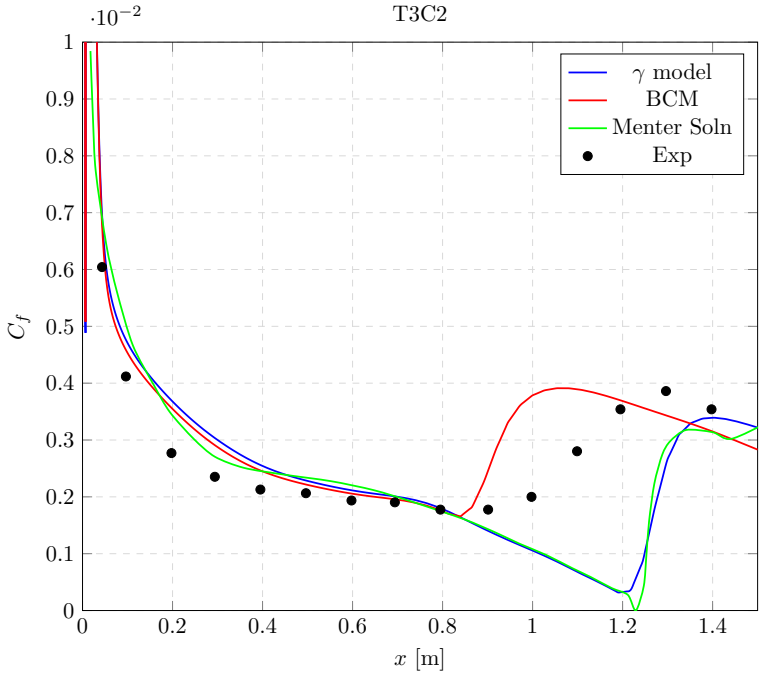

Figure 3.16: Skin Friction Coefficients obtained with Different Models for T3C2 Case

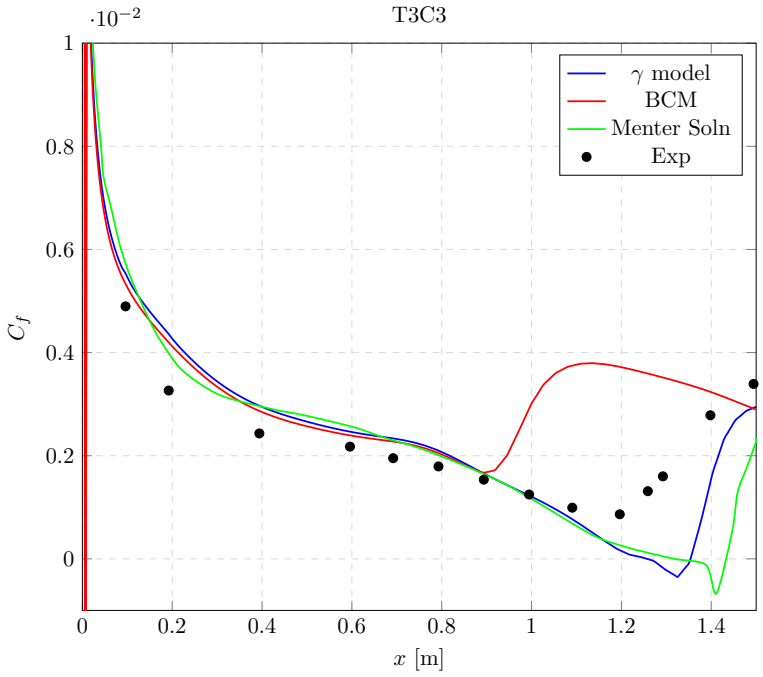

Figure 3.17: Skin Friction Coefficients obtained with Different Models for T3C3 Case

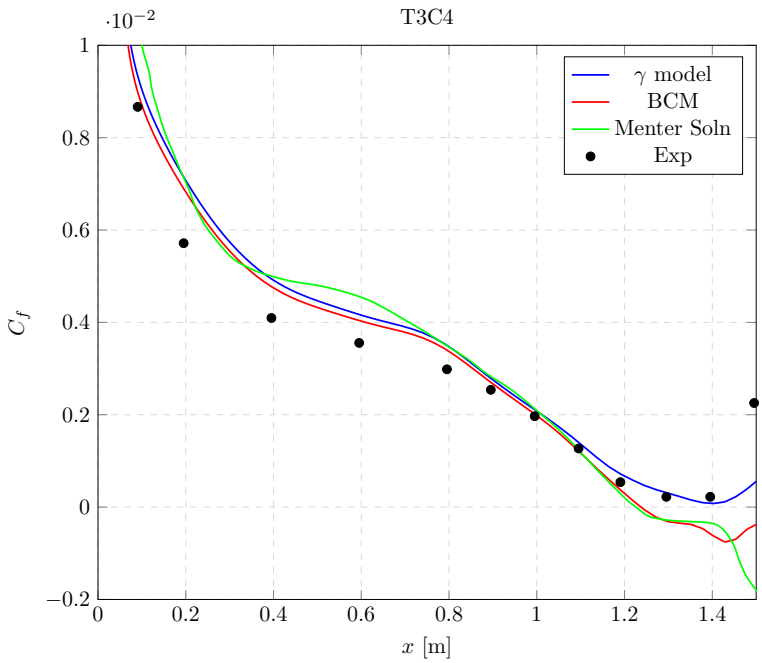

Figure 3.18: Skin Friction Coefficients obtained with Different Models for T3C4 Case

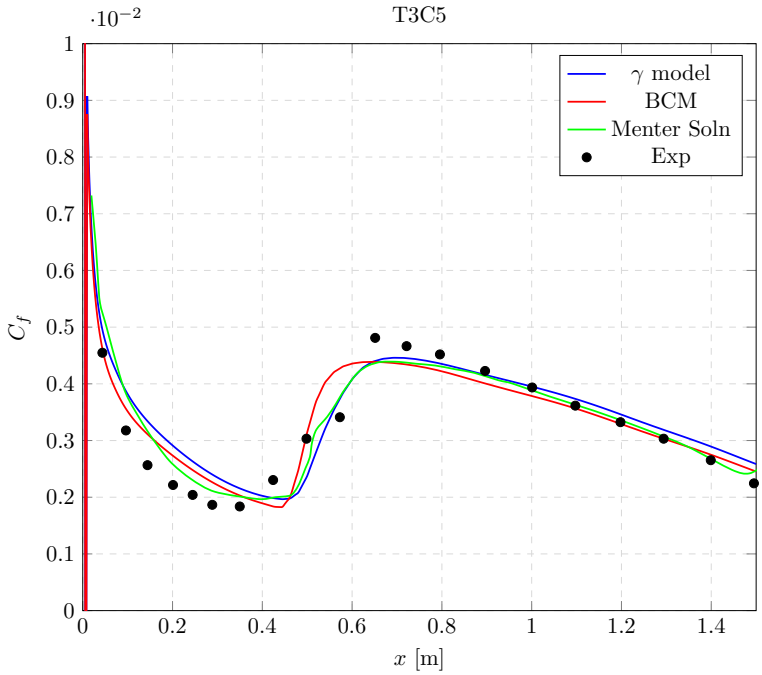

Figure 3.19: Skin Friction Coefficients obtained with Different Models for T3C5 Case

In the T3C2 case, both transition models capture transition onset with some error. Both models predict a good enough skin friction coefficient after flow becomes fully turbulent. The Menter one-equation γ model and Bas-Cakmakciglu Model predict transition reasonably accurately in T3C3, similar to T3C2. T3C4 is the case with the smallest velocity. Although both models overpredict skin friction in the laminar region, they resolve transition onset accurately. Finally, in the T3C5 case, both transition models accurately resolve the laminar region, transition onset and length and flow after the transition. To sum up, the Menter one-equation γ model and Bas-Cakmakciglu model predict transition onset and length similar to each other, and results were reasonably accurate in favorable pressure gradient test cases.

3.2 2D Airfoil Cases

3.2.1 E387 Airfoil

Eppler E387 airfoil was tested to assess the γ model performance on 2D airfoil cases. Figure 3.20 shows the airfoil profile, which allows for a substantial amount of laminar flow before the transition on the suction side. Experimental data was taken from the study conducted at Langley low-turbulence pressure tunnel (LTPT) [28] at Reynolds number 2×10^5. Lift and drag coefficients at different angles of attack obtained in the experiments are available. The importance of this airfoil is that the laminar separation bubble is formed at the suction side, and flow reattaches as turbulent. In other words, a separation-induced transition is observed at the E387 airfoil.

A 699×179 O-type grid with a 1.075 growth ratio is generated for simulations. The first layer thickness is assigned 1×10^{-5} units to the first cell to maintain $y+ < 1$ and resolve the boundary layer accurately. Freestream turbulence intensity is specified as 0.18, and the viscosity ratio was chosen as 2. The computational grid used around the airfoil is given in figure 3.21.

In figure 3.22, numerical results obtained with the γ model are compared with experimental data. As seen in this figure, the lift and drag coefficients obtained are in good

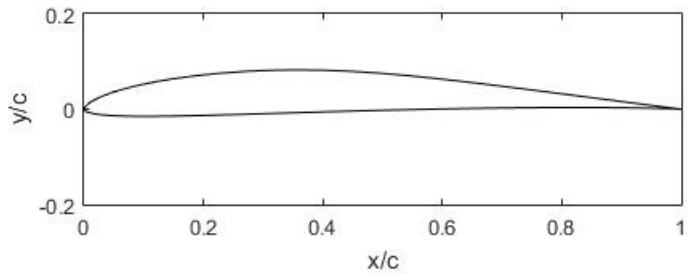

Figure 3.20: E387 airfoil profile

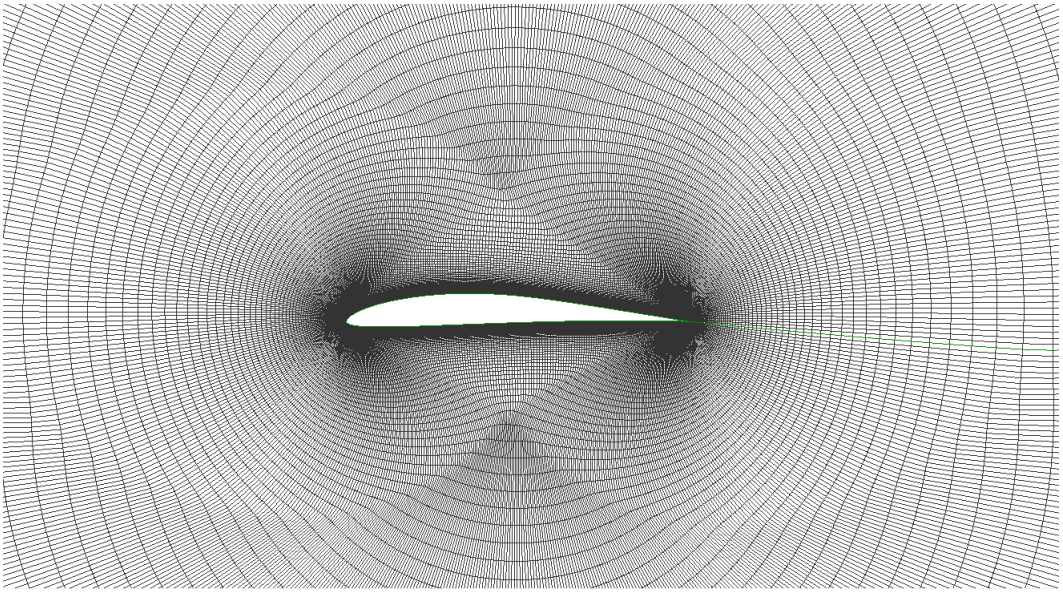

Figure 3.21: Computational domain around the E387 airfoil

agreement with experimental data, whereas a fully turbulent solution overpredicts the drag coefficients. The difference between the experimental data and simulation results at high angles of attack could be solver-based.

The importance of the E387 airfoil is that separation-induced transition occurs at the suction side of the airfoil. As expected, a fully turbulent solution misses the separation bubble. On the other hand, the γ model predicts the flow that separates the laminar and reattaches fully turbulent after the separation bubble.

It can be inferred from figure 3.23 that the γ model captures the separation bubble, whereas the fully turbulent solution misses it. The same fact can be seen in figure 3.24 also. In figure 3.24, pressure coefficients obtained with the γ model, Bas- Cakmak-

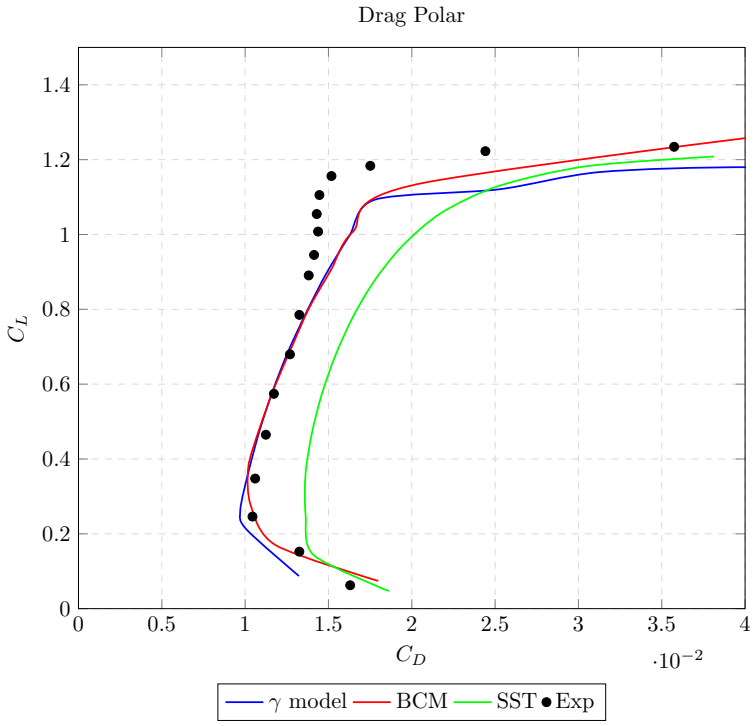

Figure 3.22: Drag polar of E387 airfoil

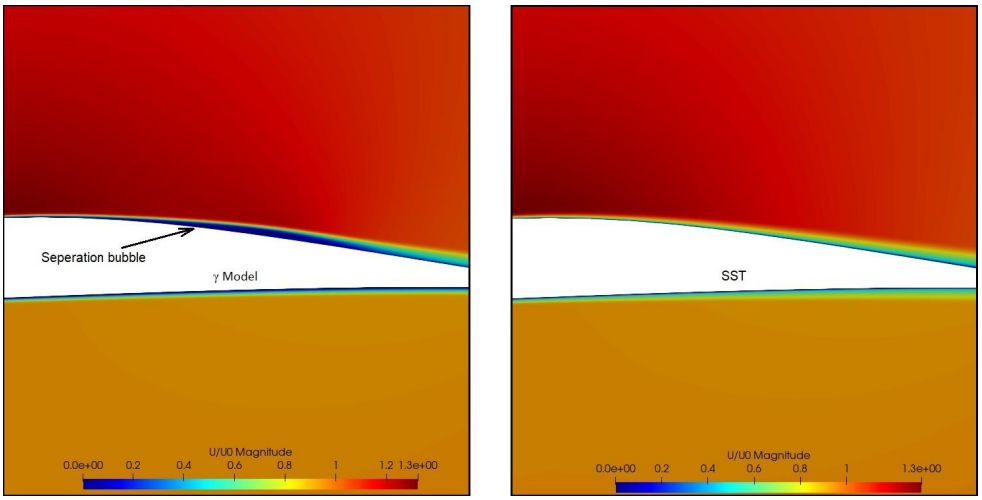

Figure 3.23: Flow field around the E387 airfoil

cioglu model and SST are presented. Both transition models capture the separation-induced transition well enough, whereas a fully turbulent solution cannot capture it.

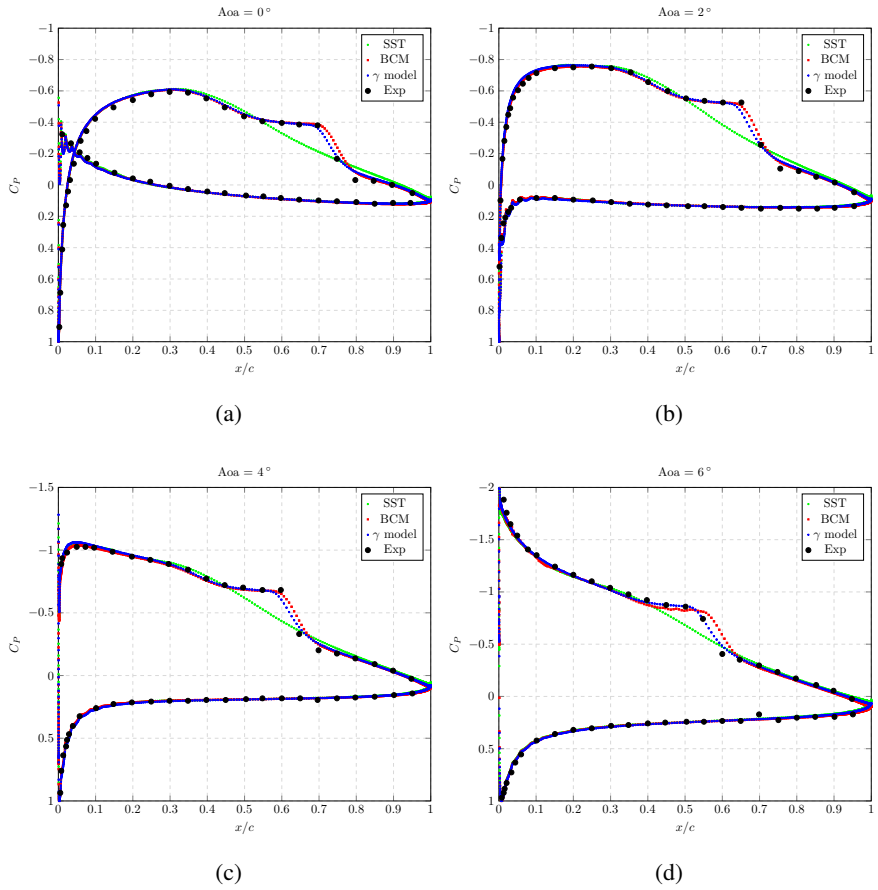

Figure 3.24: Comparison of Pressure Coefficients obtained with different models at different angles of attack

3.2.2 S809 Airfoil

The S809 airfoil is a laminar flow profile airfoil designed for horizontal axis wind turbine applications. Detailed experimental data, including drag coefficient, lift coefficient and pressure distribution of S809 airfoil, is available[29]. The airfoil profile is shown in figure 3.25.

C-type grid mesh is generated around the S809 airfoil with approximately 900 nodes (450 nodes on each side) around the airfoil. 100 nodes are created normal to airfoil profile with first layer thickness equal to 1×10^{-5} units to obtain $y+ < 1$. The farfield boundary was located ten chord lengths from the airfoil. The computational domain used can be seen in figure 3.26. Inlet conditions are given in table 3.2.

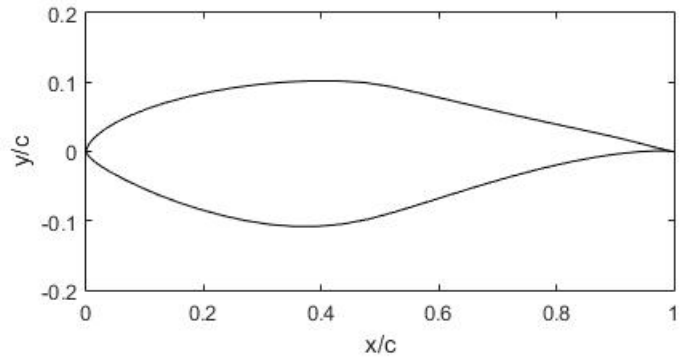

Figure 3.25: S809 airfoil profile

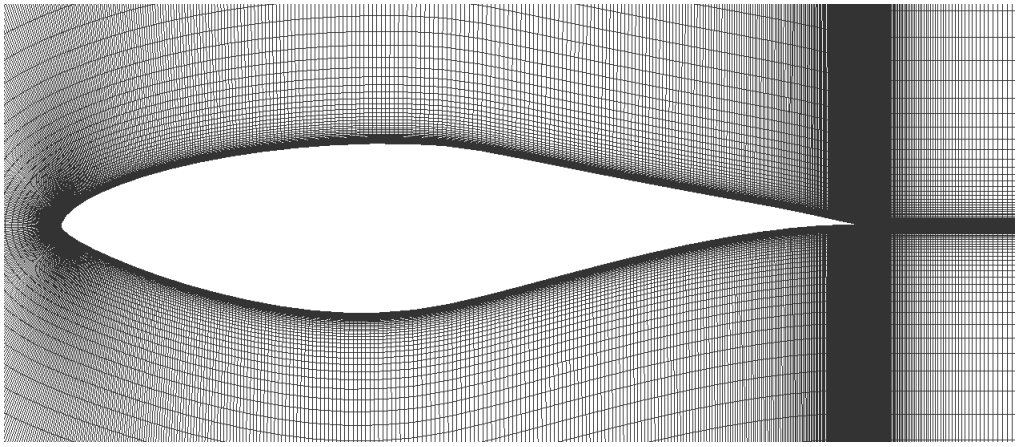

Figure 3.26: Computational domain around the S809 airfoil

Table 3.2: Inlet Conditions for the S809 Simulations

Case	Re_x	$Mach$	$Chord(m)$	$FSTI($	μ_t/μ	α
$S809$	2×10^6	0.1	1	0.05	10	$0 \circ to 14 \circ$

Drag polar of S809 airfoil at various angles of attacks are given in figure 3.28. Transition models significantly improve the drag coefficient prediction since the effect of laminar flow over the airfoil surface is captured. Menter's one-equation γ model and the Bas-Cakmakcioglu model make similar predictions.

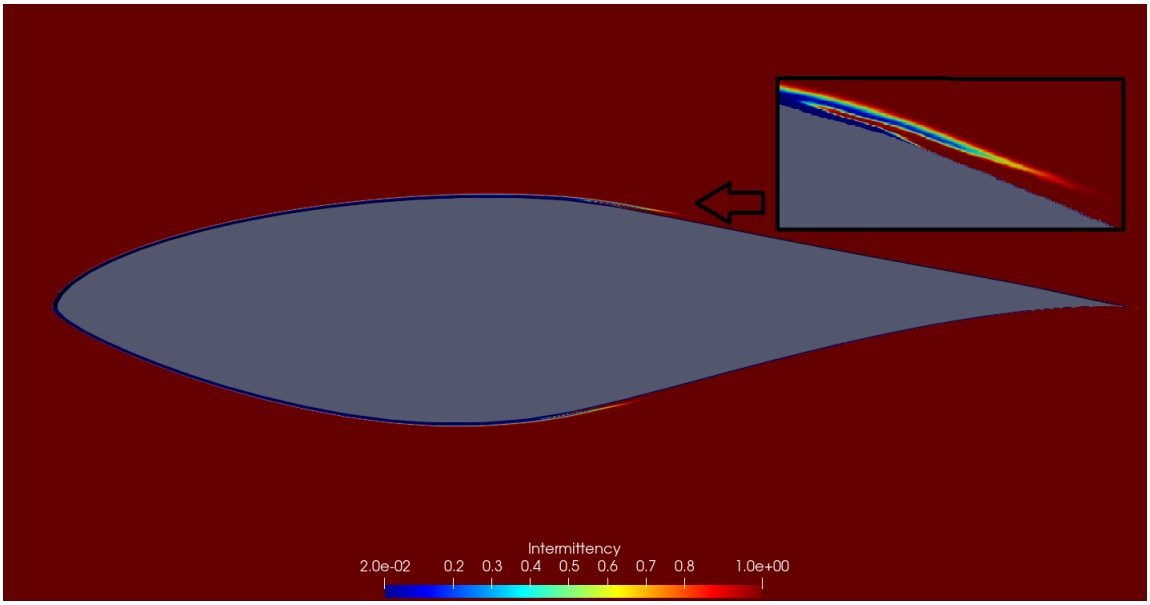

Figure 3.27: Intermittency at the angle of attack of $\alpha = 1\circ$

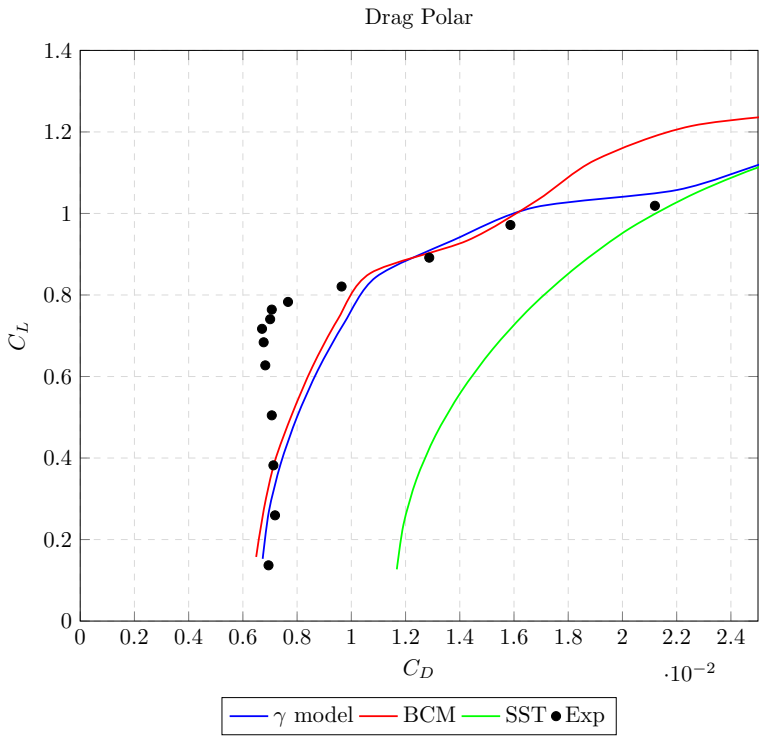

Figure 3.28: Drag polar of S809 Airfoil

3.3 Importance of Freestream Turbulence Properties

The most important drawback of Menter's one equation γ model is its sensitivity to the inlet turbulence intensity and viscosity ratio, whose determination is the source of

uncertainty [8]. The model can predict different transition characteristics in transition onset and length for different inlet turbulence intensity and viscosity ratios. The most important reason for this behavior is the underlying turbulence model, $k-\omega$ SST. The intermittency γ is coupled with the turbulent kinetic energy, hence the turbulence intensity. Therefore γ model is affected by local turbulence characteristics. However, the success of the BC model shows that the turbulence intensity at the leading edge of the plate is the critical factor for transition onset. Notice that the underlying turbulence model of BCM, Spalart-Allmaras, does not provide any turbulence information.

On the other hand, in external flow simulations, a user must provide appropriate k and ω boundary conditions at the freestream to solve transitions accurately. The k can be determined relatively easily. However, it is difficult to determine ω in engineering problems.

In order to show this dependence on freestream conditions, the Menter one-equation γ model is tested for different freestream turbulence properties T3A test case.

Note that the freestream turbulence intensity alters the transition onset, and for all test cases, this parameter is measured and reported. Therefore, the freestream turbulence intensity is kept the same with the experimental data while the viscosity ratio changes. Applied freestream turbulence properties are presented in table 3.3.

Table 3.3: Applied Values of Inlet Viscosity Ratio

	μ_t/μ						
$Setup$	1	4	9	12	30	60	120

Response of Menter one equation γ model to different viscosity ratios is given in figure 3.29.

Figure 3.29 shows that the freestream viscosity ratio has a significant effect on the results. For $\mu_t/\mu = 1$, flow behaves completely laminar. An increase in the viscosity ratio results in transition onset location moving closer to the leading edge of the plate.

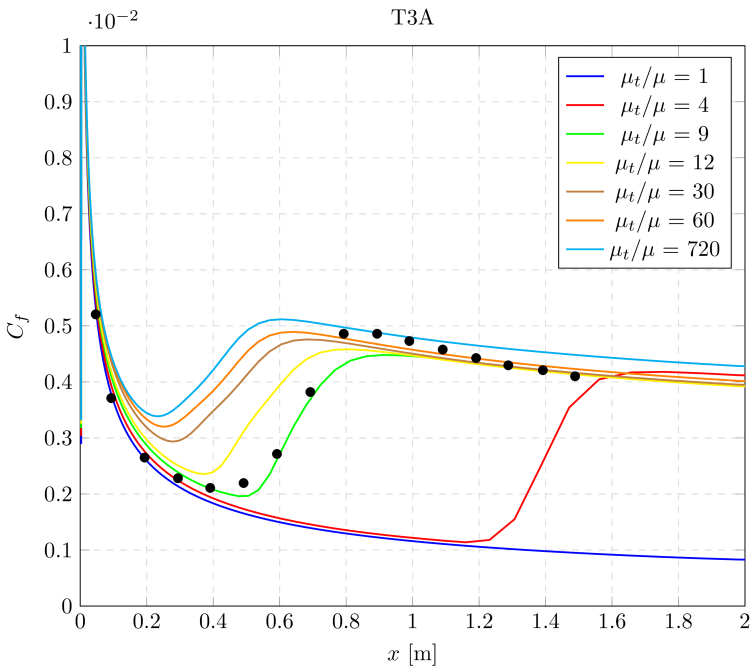

Figure 3.29: Effect of the viscosity ratio of freestream inlet conditions

3.4 Discussion

In general, the Menter one equation γ model results were in good agreement with experimental data for different test cases. In this thesis, the γ model is tested for a natural transition, bypass transition with and without pressure gradient and separation-induced transition. The model can predict natural transition accurately and bypass transition with reasonable accuracy. Zero pressure gradient test case simulations show that the success of the model is highly dependent on the freestream turbulence properties. It should be noted that some of the freestream turbulence characteristics are difficult to determine in real-life applications. The viscosity ratio effect study showed that transition prediction could change significantly for different viscosity ratio specifications. Mentioned deficiency complicates the simulation preparation and, as a result, the applicability of the γ model to general flow cases. Nevertheless, the model can show acceptable performance if the freestream values can be specified realistically.

Zero-equation Bas-Cakmakcioglu transition model predicts transition effects similar to the γ model for different transition modes. On the other hand, the BC model does

not suffer excessive turbulence boundary conditions requirements as it only requires the freestream turbulence intensity. In addition to that, as it does not solve additional differential equations, solutions are obtained faster compared to the γ model. It should be noted that both models predict the transition onset accurately, and both of them can be applied depending on the selection of the underlying turbulence model.

CHAPTER 4

CONCLUSION

4.1 Conclusions

In this study, we have studied the Menter one-equation γ model for transitional flows. The model is implemented with an open-source CFD solver. Then, the transition model is tested on different well-known benchmark transitional cases. Before the testing process, a mesh generation study is done to assess the performance of the transitional model. Besides the Menter one equation γ model, results for mentioned test cases are obtained using Bas-Cakmakcioglu turbulence transition models. This approach aimed to verify the Menter one equation γ model by comparing it with another transition model, which was also tested. Results show that both transition models give similar predictions as long as freestream turbulence properties are specified accurately. The performance of both transition models used in this study depends on the freestream turbulence intensity. BC-model stands out as it does not suffer from the freestream viscosity ratio.

4.2 Future Work

The Menter one equation γ model is tested in this study on a flat plate and two- dimensional airfoil cases. None of the test cases were decisive for the model performance for relaminarization problems. Thus, the model can be tested for the relaminarization problem in future work. In addition to that, the success of the model could be tested on 3D geometries to assess the model's success for crossflow transition.

REFERENCES

[1] F. Menter, T. Esch, and S. Kubacki, "Transition modelling based on local variables," in *Engineering Turbulence Modelling and Experiments 5*, pp. 555–564, Elsevier, 2002.

[2] F. R. Menter, R. B. Langtry, S. Likki, Y. Suzen, P. Huang, and S. Völker, "A correlation-based transition model using local variables—part i: model formulation," 2006.

[3] R. B. Langtry, F. Menter, S. Likki, Y. Suzen, P. Huang, and S. Völker, "A correlation-based transition model using local variables—part ii: test cases and industrial applications," 2006.

[4] R. B. Langtry and F. R. Menter, "Correlation-based transition modeling for unstructured parallelized computational fluid dynamics codes," *AIAA journal*, vol. 47, no. 12, pp. 2894–2906, 2009.

[5] F. R. Menter, P. E. Smirnov, T. Liu, and R. Avancha, "A one-equation local correlation-based transition model," *Flow, Turbulence and Combustion*, vol. 95, no. 4, pp. 583–619, 2015.

[6] W. Frei, "Which turbulence model should i choose for my cfd application?," 2013.

[7] R. E. Mayle, "The 1991 igti scholar lecture: the role of laminar-turbulent transition in gas turbine engines," 1991.

[8] R. B. Langtry, "A correlation-based transition model using local variables for unstructured parallelized cfd codes," 2006.

[9] B. Aupoix, D. Arnal, H. Bézard, B. Chaouat, F. Chedevergne, S. Deck, V. Gleize, P. Grenard, and E. Laroche, "Transition and turbulence modeling," *Aerospace Lab*, no. 2, pp. p–1, 2011.

[10] J.-S. Wang and J.-J. Wang, "Wake-induced transition in the low-reynolds-number flow over a multi-element airfoil," *Journal of Fluid Mechanics*, vol. 915, 2021.

[11] F. Menter, R. Langtry, and S. Völker, "Transition modelling for general purpose cfd codes," *Flow, turbulence and combustion*, vol. 77, no. 1, pp. 277–303, 2006.

[12] A. M. O. Smith, "Transition, pressure gradient and stability theory," *Douglas Aircraft Co., Report ES 26388*, 1956.

[13] R. H. Nichols, "Turbulence models and their application to complex flows," *University of Alabama at Birmingham, Revision*, vol. 4, p. 89, 2010.

[14] W. P. Jones and B. Launder, "The calculation of low-reynolds-number phenomena with a two-equation model of turbulence," *International Journal of Heat and Mass Transfer*, vol. 16, no. 6, pp. 1119–1130, 1973.

[15] S. Dhawan and R. Narasimha, "Some properties of boundary layer flow during the transition from laminar to turbulent motion," *Journal of Fluid Mechanics*, vol. 3, no. 4, pp. 418–436, 1958.

[16] U. Kaynak, O. Bas, S. C. Cakmakcioglu, and I. H. Tuncer, "Transition modeling for low to high speed boundary layer flows with cfd applications," in *Boundary layer flows-theory, applications and numerical methods*, intechopen, 2019.

[17] Y. Suzen and P. Huang, "An intermittency transport equation for modeling flow transition," in *38th Aerospace Sciences Meeting and Exhibit*, p. 287, 2000.

[18] D. K. Walters and D. Cokljat, "A three-equation eddy-viscosity model for reynolds-averaged navier–stokes simulations of transitional flow," *Journal of fluids engineering*, vol. 130, no. 12, 2008.

[19] S. C. Cakmakcioglu, O. Bas, and U. Kaynak, "A correlation-based algebraic transition model," *Proceedings of the Institution of Mechanical Engineers, Part C: Journal of Mechanical Engineering Science*, vol. 232, no. 21, pp. 3915–3929, 2018.

[20] J. Steelant and E. Dick, "Modeling of laminar-turbulent transition for high freestream turbulence," *J. Fluids Eng.*, vol. 123, no. 1, pp. 22–30, 2001.

[21] J. R. Cho and M. K. Chung, "Ak—ε—γ equation turbulence model," *Journal of Fluid Mechanics*, vol. 237, pp. 301–322, 1992.

[22] F. R. Menter, "Two-equation eddy-viscosity turbulence models for engineering applications," *AIAA journal*, vol. 32, no. 8, pp. 1598–1605, 1994.

[23] S. C. Cakmakcioglu, O. Bas, R. Mura, and U. Kaynak, "A revised one-equation transitional model for external aerodynamics," in *AIAA Aviation 2020 Forum*, p. 2706, 2020.

[24] H. W. Emmons, "The laminar-turbulent transition in a boundary layer-part i," *Journal of the Aeronautical Sciences*, vol. 18, no. 7, pp. 490–498, 1951.

[25] G. B. Schubauer and P. S. Klebanoff, "Contributions on the mechanics of boundary-layer transition," tech. rep., 1955.

[26] A. Savill, "Some recent progress in the turbulence modelling of by-pass transition," *Near-wall turbulent flows*, pp. 829–848, 1993.

[27] E. Luke, X. Tong, and R. Chamberlain, "Flowpsi: An ideal gas flow solver-the user guide," *epub*, pp. 29–40, 2016.

[28] R. J. McGhee, *Experimental results for the Eppler 387 airfoil at low Reynolds numbers in the Langley low-turbulence pressure tunnel*, vol. 4062. National Aeronautics and Space Administration, Scientific and Technical . . . , 1988.

[29] D. M. Somers, "Design and experimental results for the s809 airfoil," tech. rep., National Renewable Energy Lab.(NREL), Golden, CO (United States), 1997.

[30] W. Willmarth, "Structure of turbulence in boundary layers," *Advances in applied mechanics*, vol. 15, pp. 159–254, 1975.

[31] S. B. Pope and S. B. Pope, *Turbulent flows*. Cambridge university press, 2000.

[32] H. Schlichting and K. Gersten, *Boundary-layer theory*. Springer Science & Business Media, 2003.

[33] O. Bas, S. C. Cakmakcioglu, and U. Kaynak, "A novel intermittency distribution based transition model for low-re number airfoils," in *31st AIAA applied aerodynamics conference*, p. 2531, 2013.

[34] P. Malan, K. Suluksna, and E. Juntasaro, "Calibrating the gamma-re_theta transition model for commercial cfd," in *47th AIAA Aerospace Sciences Meeting Including The New Horizons Forum and Aerospace Exposition*, p. 1142, 2009.

[35] E. Juntasaro, K. Ngiamsoongnirn, P. Thawornsathit, and P. Durbin, "Development of an intermittency transport equation for modeling bypass, natural and separation-induced transition," *Journal of Turbulence*, vol. 22, no. 9, pp. 562–595, 2021.

[36] E. Juntasaro and A. A. Narejo, "A gamma-kl transition model for transitional flow with pressure gradient effects," *Engineering Journal*, vol. 21, no. 2, pp. 279–304, 2017.

[37] S. Medida, *Correlation-based transition modeling for external aerodynamic flows*. PhD thesis, University of Maryland, College Park, 2014.

[38] S. Medida and J. Baeder, "Application of the correlation-based gamma-re theta t transition model to the spalart-allmaras turbulence model," in *20th AIAA computational fluid dynamics conference*, p. 3979, 2011.

[39] S. Schmidt and F. Thiele, "Detached eddy simulation of flow around a-airfoil," *Flow, turbulence and combustion*, vol. 71, no. 1, pp. 261–278, 2003.

[40] J. Fürst, P. Straka, J. Příhoda, and D. Šimurda, "Comparison of several models of the laminar/turbulent transition," in *EPJ Web of Conferences*, vol. 45, p. 01032, EDP Sciences, 2013.

[41] V. D'Alessandro, S. Montelpare, and R. Ricci, "Assessment of a spalart–allmaras model coupled with local correlation based transition approaches for wind turbine airfoils," *Applied Sciences*, vol. 11, no. 4, p. 1872, 2021.

[42] U. Kujansuu *et al.*, "Implementation of a one-equation local correlation-based transition model," 2017.

[43] M. J. Collison, P. X. Harley, and D. di Cugno, "Experimental and numerical investigation of transition effects on a low reynolds number airfoil," in *Turbo Expo: Power for Land, Sea, and Air*, vol. 50794, p. V02BT41A008, American Society of Mechanical Engineers, 2017.

[44] G. Rubino, *Laminar-to-Turbulence Transition Modeling of Incompressible Flows in a RANS Framework for 2D and 3D Configurations*. PhD thesis, Ecole Centrale de Nantes, 2021.

[45] B. Lee and J. D. Baeder, "Prediction and validation of laminar-turbulent transition using sa-γ transition model," in *AIAA Scitech 2021 Forum*, p. 1532, 2021.

[46] K. E. Swalwell, *The effect of turbulence on stall of horizontal axis wind turbines*. PhD thesis, Monash University, 2005.

[47] Y. Zhang, Z. Zhou, K. Wang, and X. Li, "Aerodynamic characteristics of different airfoils under varied turbulence intensities at low reynolds numbers," *Applied Sciences*, vol. 10, no. 5, p. 1706, 2020.

[48] K. E. Swalwell, J. Sheridan, W. Melbourne, *et al.*, "The effect of turbulence intensity on stall of the naca 0021 aerofoil," in *14th Australasian fluid mechanics conference*, pp. 941–944, 2001.

[49] P. Bader and W. Sanz, "Measurement and simulation of a turbulent boundary layer exposed to acceleration along a flat plate," in *12 th European Conference on Turbomachinery Fluid dynamics & Thermodynamics*, EUROPEAN TURBOMACHINERY SOCIETY, 2017.

[50] C. Xia and W. Chen, "Boundary-layer transition prediction using a simplified correlation-based model," *Chinese Journal of Aeronautics*, vol. 29, no. 1, pp. 66–75, 2016.

[51] R. Langtry, J. Gola, and F. Menter, "Predicting 2d airfoil and 3d wind turbine rotor performance using a transition model for general cfd codes," in *44th AIAA aerospace sciences meeting and exhibit*, p. 395, 2006.

[52] F. Menter and R. Langtry, "Transition modelling for turbomachinery flows," *Low Reynolds Number Aerodynamics and Transition*, pp. 31–58, 2012.

[53] R. Mayle and A. Schulz, "The path to predicting bypass transition," in *Turbo Expo: Power for Land, Sea, and Air*, vol. 78729, p. V001T01A065, American Society of Mechanical Engineers, 1996.

[54] F. R. Menter, M. Kuntz, and R. Langtry, "Ten years of industrial experience with the sst turbulence model," *Turbulence, heat and mass transfer*, vol. 4, no. 1, pp. 625–632, 2003.

[55] W. S. Saric, H. L. Reed, and E. J. Kerschen, "Boundary-layer receptivity to freestream disturbances," *Annual review of fluid mechanics*, vol. 34, no. 1, pp. 291–319, 2002.

[56] C. Müller and F. Herbst, "Modelling of crossflow-induced transition based on local variables," *Proc. ECCOMAS, Paper*, no. 2252, p. 72, 2014.

[57] D. K. Walters and J. H. Leylek, "A new model for boundary layer transition using a single-point rans approach," *J. Turbomach.*, vol. 126, no. 1, pp. 193–202, 2004.

[58] "Turbulence modeling resource."